

# FastCTM (v1.0): Atmospheric chemical transport modelling with a principle-informed neural network for air quality simulations

Baolei Lyu<sup>1,2,3</sup>, Ran Huang<sup>4,5</sup>, Xinlu Wang<sup>4</sup>, Weiguo Wang<sup>6</sup>, Yongtao Hu<sup>7</sup>

<sup>1</sup> Huayun Sounding Meteorological Technology Co. Ltd., Beijing 102299, China

<sup>2</sup> Key Laboratory of Intelligent Meteorological Observation Technology, Beijing 100081, China

<sup>3</sup> China Meteorological Administration Xiong'an Atmospheric Boundary Layer Key Laboratory, Xiong'an, 071000, China

<sup>4</sup> Hangzhou AiMa Technologies, Hangzhou, Zhejiang 311121, P. R. China

<sup>5</sup> Nanjing AiMa Environmental, Nanjing, Jiangsu 210000, P. R. China

<sup>6</sup> SAIC, at Environment Modelling Center, NOAA/National Centers for Environmental Prediction, College Park, Maryland 20740, United States

<sup>7</sup> School of Civil and Environmental Engineering, Georgia Institute of Technology, Atlanta, Georgia 30332, United States

Correspondence to: Baolei Lyu (baoleilv@foxmail.com), Ran Huang (ranhuang2019@163.com)

**Abstract.** Chemical-transport models (CTM) have wide and profound applications in CTMs are indispensable for air-quality simulation and management. However, its applications are often constrained assessment and policy development, yet their operational use is hampered by high computational burdens. In this study, we developed cost. We present FastCTM, a physics-informed neural-network based CTM model (FastCTM) to efficiently simulate emulator that rapidly predicts hourly concentrations of ten airkey pollutant composition variables, including major  $PM_{2.5}$  species of  $SO_4^{2-}$ ,  $NO_3^-$ ,  $NH_4^+$ ,  $(SO_4^{2-}, NO_3^-, NH_4^+)$ , organic matters and other inorganic components, matter, elemental carbon, crustal material), coarse part of  $PM_{10}$ ,  $SO_2$ ,  $NO_2$ ,  $PM_{10}$ ,  $SO_2$ ,  $NO_2$ ,  $CO$ , and  $O_3$ . The  $O_3$ . FastCTM has a principle-informed structure by explicitly encoding atmospheric physical and chemical processes in a basic simulator. Specifically, in the simulator, embeds five process-specific neural network modules are proposed to respectively represent five major atmospheric processes of primary emissions, horizontal transport, turbulent diffusion, chemical reactions and depositions. deposition within a unified framework. Given 1-hour initial condition data, the FastCTM is able to can simulate future 24-hour concentrations of thefor ten air pollutants withusing corresponding meteorology-meteorological fields and emissions as input. The FastCTM is trained with operational forecast data from a numerical CTM model named Community Multiscale Air Quality (CMAQ) in Trained on 2018–2022. The well-trained FastCTM is- WRF-CMAQ forecasts over China and evaluated comparing to the long-term on 2023 data, FastCTM reproduces CMAQ forecast in an independent year 2023, and achieves high-agreements with mean RMSE values ( $\mu g\ m^{-3}$ ) of 9.1, 11.9, 4.4, 4.0, 48.9 and 10.9  $\mu g/m^3$  and  $R^2$ -values  $R^2$  of 0.880, 0.81, 0.880, 0.83, 0.9 and 0.770 for  $PM_{2.5}$ ,  $PM_{10}$ ,  $SO_2$ ,  $NO_2$ ,  $PM_{2.5}$ ,  $PM_{10}$ ,  $SO_2$ ,  $NO_2$ ,  $CO$ , and  $O_3$ . The FastCTM model also exhibited reasonable and  $O_3$ , respectively. Sensitivity tests confirm physically plausible responses of air quality to meteorological variables of air-to temperature, wind speed and planetary boundary-layer height, as well as to input pollutant and precursor emissions. Furthermore, due to the principles-oriented structure, internal chemical and physicalThe modular architecture enables quantitative process analysis could be performed by FastCTM to quantify the specific contribution from each of the five processes for hourly air pollutant concentration changes, offering CTM-like insight at GPU-accelerated speeds. In a nutshell, FastCTM has multi-functional advantages in air pollutant concentration provides a computationally efficient solution for air-quality simulations, sensitivity analysis, and internal-process analysis attribution

设置了格式: 英语(美国)

设置了格式: 英语(美国)

设置了格式: 英语(美国)

设置了格式: 英语(美国)

设置了格式: 英语(美国)

设置了格式: 英语(美国)

设置了格式: 英语(美国)

设置了格式: 英语(美国)

设置了格式: 英语(美国)

设置了格式: 英语(美国)

设置了格式: 英语(美国)

设置了格式: 英语(美国)

设置了格式: 英语(美国)

设置了格式: 英语(美国)

设置了格式: 英语(美国)

设置了格式: 英语(美国)

设置了格式: 英语(美国)

设置了格式: 英语(美国)

设置了格式: 英语(美国)

设置了格式: 英语(美国)

设置了格式: 英语(美国)

设置了格式: 英语(美国)

设置了格式: 英语(美国)

设置了格式: 英语(美国)

设置了格式: 英语(美国)

设置了格式: 英语(美国)

设置了格式: 英语(美国)

设置了格式: 英语(美国)

设置了格式: 英语(美国)

设置了格式: 英语(美国)

设置了格式: 英语(美国)

设置了格式: 英语(美国)

设置了格式: 英语(美国)

设置了格式: 英语(美国)

设置了格式: 英语(美国)

设置了格式: 英语(美国)

设置了格式: 英语(美国)

设置了格式: 英语(美国)

设置了格式: 英语(美国)

设置了格式: 英语(美国)

设置了格式: 英语(美国)

with high ~~computation efficiencies on GPU and~~ accuracy and physical consistency.

## 1 Introduction

Effective air quality management requires an accurate ~~understanding~~ characterization of air current and future pollution conditions ~~in current time and future to take~~ implement targeted emission ~~cut and~~ control measures (Wang et al., 2010; Council, 2004). Driven by this demand, deterministic air quality ~~numerien~~numerical models have been developed to simulate the spatiotemporal ~~varianees~~variability and ~~evolutionsevolution~~ of ambient air pollutants in the atmosphere (Hakami et al., 2003; Eder et al., 2006). In these models, such as the Community Multiscale Air Quality (CMAQ) model, atmospheric physical and chemical processes (e.g., emissions, chemical ~~reactionreactions~~, horizontal advection, and diffusion ~~etc.~~) are mathematically ~~defined~~represented by partial differential equations. The air pollutant and species concentrations can ~~be~~ then ~~be~~ calculated by solving these ~~complicated~~complex equations ~~with numerieusing~~ numerical methods (Byun and Schere, 2006), which is often time-consuming (Leal et al., 2017) and requires ~~intensesubstantial~~ computational resources such as high-performance computing (Efsthathiou et al., 2024).

~~Recent developments in deep~~Deep learning models ~~provideoffers~~ promising ~~alternative pathways to build fast and~~ alternatives for developing rapid, data-driven deep learning-based CTM models, owing to CTMs by leveraging the strong ~~capabilitiescapacity~~ of neural networks ~~in encoding and representingto encode~~ complex features, spatiotemporal patterns ~~and relationships that could be learned from long-term and large-size data datasets~~ (Lecun et al., 2015; He et al., 2016; Liao et al., 2020). ~~Such~~These deep learning-based CTM models are expected to provide accurate simulations that are comparable to the current deterministic ~~numerien~~numerical CTMs ~~but withwhile offering~~ much higher computational efficiency and ~~better learnableenhanced learning~~ capabilities. However, ~~related advances have progress has~~ been ~~limited due to difficultieshindered by challenges~~ in designing proper neural network structures ~~toarchitectures that~~ simultaneously achieve ~~the goals of high accuracies, structural interpretationsaccuracy, interpretability, and long-term simulations~~simulation stability and fidelity (Reichstein et al., 2019; Irrgang et al., 2021). ~~In the constructions ofconstructing~~ deep learning-based CTM models, air quality ~~simulations and predictions were always viewed~~ modeling is often formulated as a sequence-to-sequence prediction ~~problemsproblem~~ (Shi et al., 2015; Zhang et al., 2024) to ~~modelcapture~~ the spatiotemporal correlations among multiple variables. ~~Therefore~~Consequently, previous studies ~~have~~ mainly focused on refining ~~theneural network's~~ representation capabilities ~~of the neural network~~ by proposing new neural-network operations and structures to improve error back-propagation efficiencies and model encoding capabilities (Wang et al., 2018; Huang et al., 2021; Mao et al., 2021). For example, Xing et al. (2022) developed a deep learning-based module named deepCTM ~~through mimiekingthat~~ mimics atmospheric photochemical modeling to simulate ozone concentrations. However, these deep learning-based CTMs are often structured ~~in anas~~ uninterpretable black-box ~~style tomodels that~~ generate simulations ~~that reflectreflecting~~ the cumulative effect of all physical and chemical processes. ~~These~~Such black-box models ~~have limitations in modellinghinder~~ error attribution, ~~inspection of~~ internal processes ~~inspection~~ and knowledge ~~findings etc. discovery~~ (Reichstein et al., 2019). Quantifying individual ~~atmospheric~~ processes ~~would provide fundamental explanations forenables~~ a model's ~~mechanistic interpretation of model~~ predictions; and ~~therefore is also useful in identifying potential sourcesidentification~~ of error ~~in the model formulation or its inputsources~~ (Liu et al., 2010). ~~With the motivation, there are~~ Motivated by this need, recent studies ~~dedicated to develop model tohave~~ developed models that learn one-specific atmospheric ~~proecess, i.e. processes,~~ such as chemical ~~reactions~~ and deposition, ~~in thewithin~~ CTM ~~modelframeworks~~. Kelp et al. (2022) developed a neural network chemical solver for stable long-term global simulations of atmospheric chemistry, ~~learned~~trained from the GEOS-

设置了格式: 英语(美国)

设置了格式: 英语(美国)

Chem model. Xia et al. (2024) simulated 74 chemical species and 229 reactions following the SAPRC-99 mechanism ~~with using~~ an artificial intelligence photochemistry (AIPC) scheme ~~to achieve~~, achieving approximately 8-time-fold speed-up. Sturm and Wexler (2020) developed a mass- and energy-conserving framework for using machine learning to ~~speed accelerate~~ computations ~~with an~~, demonstrating successful application in a photochemistry example. For the deposition process, Silva et al. (2019) proposed a deep learning parameterization for ozone dry deposition velocities ~~with that provided~~ accurate predictions ~~in on~~ independent new ~~date sets~~ datasets, revealing the potential of neural ~~network in~~ ~~encoding networks to capture~~ complex spatio-temporal latent processes. Liu et al. (2025) proposed a Neural Network Emulator, named ChemNNE, for ~~fast rapid~~ chemical concentration modelling, which achieved ~~good strong~~ performance in both accuracy and efficiency. ~~Even though/Although~~ these ~~successful applications using deep learning methods to simulate individual atmospheric chemical and physical processes, there is an missing~~ successes, a gap ~~remains~~ in coupling these NN ~~operator replacements together as an~~ operators into a complete deep-learning-based CTM.

The main objective of our study is to ~~build develop~~ and validate a principles-guided, neural network-based FastCTM ~~that could simulate, capable of simulating~~ spatial-temporal fields of hourly concentrations of major air pollutant species ~~like in the same manner as~~ a traditional CTM. FastCTM ~~could can~~ model individual contributions from each ~~of the~~ atmospheric ~~processes of process~~: transport, diffusion, deposition, ~~reaction~~ chemical reactions, and ~~emission~~ emissions. FastCTM is currently configured to simulate hourly concentrations of 10 criteria pollutants ~~critical for~~ relevant to health impact assessment and policy-making, including ~~and~~ major species of PM<sub>2.5</sub> (SO<sub>4</sub><sup>2-</sup>, NO<sub>3</sub><sup>-</sup>, NH<sub>4</sub><sup>+</sup>, organic matters and other inorganic components, coarse part in PM<sub>10</sub>, CO, NO<sub>2</sub>, SO<sub>2</sub>, and O<sub>3</sub>). ~~Interpretations~~ Enhancing the interpretability of deep-learning ~~network are also widely vowed to improve~~ models is critical for advancing their ~~applications~~ application in ~~earth~~ Earth system science ~~and, including both climate studies and air-quality research~~. The well-trained FastCTM model is capable of performing analysis of internal chemical and physical processes. The FastCTM model ~~would bring~~ offers many benefits ~~with their, including~~ high ~~computation~~ computational speed, efficient data assimilation, and ~~fast rapid~~ model updates.

## 2 Data and Methods

### 2.1 Parent Model Simulations and Datasets

In this study, the FastCTM model was designed to replicate the parent model CMAQ, trained by learning CMAQ's underlying physical and chemical processes among multiple air pollutants, including the complicated chemical reaction, transport, diffusion, and deposition. CMAQ has a process analysis (PA) tool to separate out and quantify the contributions of individual physical and chemical processes to the changes in the predicted concentrations of a pollutant, which ~~provide~~ provides the opportunity to conduct a sensitivity analysis by comparing process contributions between CMAQ and FastCTM.

~~The weather~~ Weather and air quality simulations ~~in from~~ 2018~ to 2023 were conducted using a WRF-CMAQ ~~modelling~~ modeling system ~~that consists~~ consisting of three major components: ~~The~~ (1) the meteorology component ~~of, the~~ Weather Research and ~~Forecast~~ Forecasting model ~~(, WRF, v3.4.1)~~ (Michalakes et al., 2005; Skamarock et al., 2008), ~~which~~ provides meteorological fields, ~~the; provides meteorological fields,~~ (2) the emission component ~~provides, which supplies~~ gridded estimates of hourly ~~emission~~ emission rates ~~offor~~ primary pollutants ~~that~~ matched to model species, and (3) the CTM component ~~(, CMAQ v5.0.2 (Byun and Schere, 2006))~~, ~~which~~ solves the governing physical and chemical equations to obtain 3-D pollutant ~~concentrations~~ concentration fields. WRF-CMAQ simulations are not two-way coupled, so ~~that~~

weather and chemistry ~~and chemistry~~ do not ~~have feedbacks to~~ influence each other. We used hourly average concentrations of dominant PM<sub>2.5</sub> components of sulfate (SO<sub>4</sub>), nitrate (NO<sub>3</sub>), ammonium (NH<sub>4</sub>), organic carbon (OC<sub>2</sub>), and other components (EC and soil, etc.), and CO, SO<sub>2</sub>, NO<sub>2</sub>, and O<sub>3</sub> in the surface layer. The 10 species were selected based on their direct relevance to regulatory standards (e.g., PM<sub>2.5</sub>, PM<sub>10</sub>, O<sub>3</sub>, NO<sub>2</sub>, SO<sub>2</sub>, and CO) and their dominance in driving health and environmental impacts in urban and industrial regions.

Meteorological variables used in this study include relative humidity (RH), air temperature (T), wind components (U, V) at surface 10 meters height, precipitation (RN), cloud fraction (CFRAC<sub>2</sub>), and planetary boundary layer height (PBLH). Wind speed (WS) was calculated from U and V. The data covered the whole of China at a horizontal resolution of ~~12 km~~ 1.2 km with 372×426 grid cells. The simulation data ~~off from~~ 2018--2022 is ~~are~~ used as the training dataset, while the remaining simulation data in 2023 is used for independent evaluation. The surface topographic data (HGT, Figure S1 in the supplementary material, obtained from <https://data.cr.usgs.gov/GTOPO30>) and land cover data (Zhang et al., 2020) of urban and tree fraction (LULC) are also used to reflect the effects of land surface conditions in this study.

The original primary emissions used in the aforementioned WRF-CMAQ modelling system are used as input to the FastCTM. The large amount of emission data is grouped according to the simulated 10 pollutant variables. Specifically, the primary PM<sub>2.5</sub> emissions of SO<sub>4</sub>, NO<sub>3</sub>, NH<sub>4</sub>, OC<sub>2</sub>, and other components, and gaseous emissions including sulfur oxide (SO<sub>2</sub>), nitrogen oxides (NO<sub>x</sub>, including HONO, NO, and NO<sub>2</sub>), ammonia (NH<sub>3</sub>), volatile organic species (VOCs, including isoprene (ISOP), terpene (TERP), and other species of VOC) are used in the FastCTM. Annual average emission ~~emissions~~ of NO<sub>x</sub>, SO<sub>2</sub>, and VOC are respectively depicted in Figure S2-4 in the supplementary material.

## 2.2 FastCTM Model Formulations

### 2.2.1 FastCTM Model Framework

The deterministic CTM models simulate emissions, transport, deposition, diffusion, and chemical transformations of gases and particles in the troposphere through numerically solving the governing equations as follows,

$$\frac{\partial C_i}{\partial t} = -\nabla \cdot (\bar{u}C_i) + \nabla \cdot (K\nabla C_i) + R_i + E_i + D_i \quad (1)$$

where  $C_i$  is the concentration of species  $i$ ,  $u$  is the air fluid velocity,  $K$  is the eddy diffusivity tensor,  $R_i$  is the net rate of chemical generation of species  $i$ ,  $E_i$  is the rate of direct addition of the species from primary emissions, and  $D_i$  is the deposition rate caused by both dry and wet depositions. A detailed description of CMAQ principles is available elsewhere (Byun and Schere, 2006; Appel et al., 2017). Inspired by ~~the traditional numerical~~ numerical CTMs principles and equations, the guiding framework of FastCTM was also structured in a similar formulation to represent the dominant processes in order to simulate air pollutant spatiotemporal variations.

In the context of deep learning, hourly air quality simulation is a spatiotemporal sequence-to-sequence learning problem ~~to predict~~ aimed at predicting the most probable future length- $K$ -sequence of length  $K$ , given ~~thea~~ previous length- $J$ -sequence of length  $J$ , as shown in the following Eq.2,

$$\hat{Y}_{t+1}, \dots, \hat{Y}_{t+K} = \arg \max p \left( [Y_{t-J+1}, \dots, Y_t], [X_{t-J+1}, \dots, X_t, X_{t+1}, \dots, X_{t+K}] \right) \quad (2)$$

Where the  $\arg \max$  (short for “argument of the maximum”) function is used to find the  $p$  class with the highest predicted probability. The  $X_t \in \mathbf{R}^{M \times N \times V_X}$  is the data of  $V_X$  input variables at the spatial grid of  $M \times N$  at time  $t$ . The  $Y_t \in \mathbf{R}^{M \times N \times V_Y}$  is the data of  $V_Y$  predictive variables at time  $t$ . Specifically, the FastCTM simulates future  $K$ -hour air pollutant concentrations, given  $J$ -hour air pollutant concentrations  $[Y_{t-J+1}, \dots, Y_t]$  as initial fields and  $(K+J)$ -hour meteorological and emission conditions  $[X_{t-J+1}, \dots, X_t, X_{t+1}, \dots, X_{t+K}]$ . Previous studies generally used multiple-step input data with  $J > 1$  to

ensure sufficient spatial-temporal correlations contained in the training data (Sum et al., 2022; Xing et al., 2022). Instead, we use 1-hour initial pollutant concentration ( $J=1$ ) to simulate 24-hour air quality pollutants ( $K=24$ ), to ensure FastCTM is dedicated to ~~learn~~learning air quality changes between ~~two~~two neighboring ~~two~~two hours as shown in Figure 1a. In other words, at time  $t = 0$ , FastCTM predicted  $K$ -hour air pollutant concentrations of  $C_{t=0}, C_{t=1}, \dots, C_{t=K-1}$ , given the input air pollutant concentration in previous hour  $C_{t=-1}$  and corresponding meteorological data and emissions at time  $t = 0, 1, \dots, K-1$ . The unit of concentrations is  $\mu\text{g}/\text{m}^3$  for all pollutants.

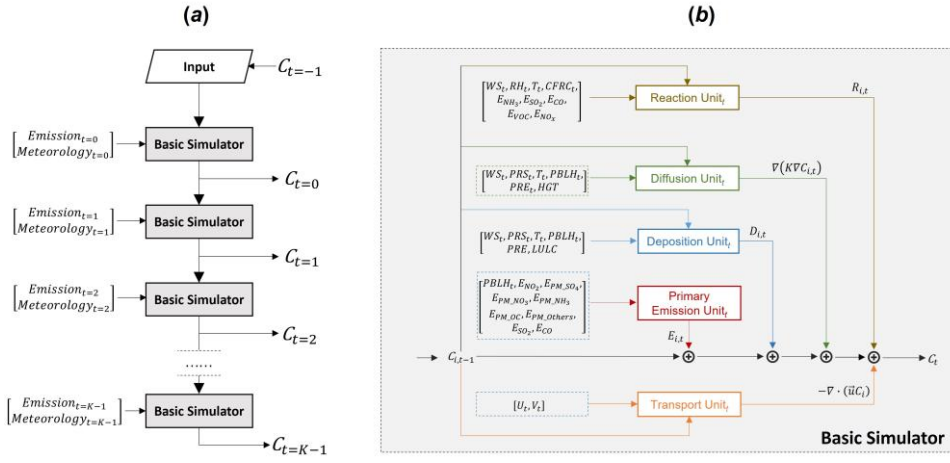


**Figure 1: (a) General model workflow, and (b) the basic simulator module structure at the time step  $t$  of the deep learning simulation model FastCTM, designed according to Eq.1. Arrows and boxes with different colours represent calculation modules of different atmospheric physical and chemical processes.**

The FastCTM model uses the basic simulator module (Figure 1a) recursively for hourly simulations, using output air pollutant concentrations from one step as input to the next-step basic simulator. In contrast to directly learning spatiotemporal correlations of predictand itself as in most previous studies (Wang et al., 2018; Shi et al., 2017), the basic simulator (Figure 1b) is formulated following the atmospheric physical and chemical equations and constraints shown in Eq.1, and ~~was~~is composed of five modules to respectively represent the physics-chemical processes to improve the model performance. The modules for each of the five processes in the basic simulator are described in the following section. The time step used in FastCTM was 60 seconds.

### 2.2.2 Primary Emissions Module

Primary pollutants are assumed to be directly emitted into the atmosphere and instantly well-mixed within the PBL. Therefore, hourly ~~enhancement of~~air-pollutant concentrations ~~enhancement~~ caused by primary emissions could be described in the following Eq.3.

$$E_{m,n,i,t} = \frac{1000 \times PE_{m,n,i,t}}{PBLH \times dx \times dy} \quad (3)$$

Where  $E_{m,n,k,t}$  refers to the concentration changes contributed by primary emissions at spatial coordinate  $(m, n)$  for species  $i$  at time  $t$ . The  $PE_{m,n,i,t}$  is the corresponding total primary emissions within the grid cell per second, which has a unit of

g/s. Considering that the cell size in the FastCTM is ~~12 km~~12km by ~~12 km~~12km, we have  $dx = 12000$  and  $dy=12000$  in this study. The boundary layer height PBLH ~~is, i~~s also in the unit of ~~meter-meters~~(m). Therefore, ~~resultedthe resulting~~ air pollutant concentration ~~increaseincreases~~ by primary emission  $E_{m,n,i,t}$  has a unit of  $\mu\text{g}/\text{m}^3$ .

### 2.2.3 Horizontal Transport Module

In the FastCTM, horizontal ~~transporttransport~~ usually ~~havehas~~ a significant influences on air quality variations (Lang, 2013). In CMAQ, the regional transport ~~was in generalis~~ generally represented ~~asby~~ the divergence of the product of wind field and air pollutant species as in Eq.1, inferred from continuity equations and convection equations (Michalakes et al., 2001; Byun and Schere, 2006). By decomposing the air mass movement into two orthogonal directions of east-west ( $x$ ) and north-south ( $y$ ), they could be ~~re-writtenrewritten~~ in the form as shown in Eq. 4,

$$\nabla \cdot (\vec{u}C_i) = \frac{\partial(C_i U)}{\partial x} + \frac{\partial(C_i V)}{\partial y} \quad (4)$$

Where the wind field ~~wasis~~ represented as  $\vec{u}$ , which ~~wasis~~ then decomposed into  $U$  and  $V$ , respectively in the  $x$  and  $y$  directions.

In the deep learning framework, the partial equation in Eq. 4 could be rewritten in a discrete form as convolution operations and inner product calculations as shown in Eq. 5 with a finite difference method. The convolutional kernels of  $W_x$  and  $W_y$  were defined in an ~~up-windupwind~~ scheme as shown in Eq. 6 and Eq. 7. ~~With the scheme, this transport module itself is mass-conserved, even though FastCTM is not mass-conserved as a whole.~~

$$\nabla \cdot (\vec{u}C_i) = \frac{W_x * (C_i * U)}{dx} + \frac{W_y * (C_i * V)}{dy} \quad (5)$$

$$W_x = \begin{cases} [-1 & 1 & 0] & \text{if } U < 0 \\ [0 & -1 & 1] & \text{if } U \geq 0 \end{cases} \quad (6)$$

$$W_y = \begin{cases} \begin{bmatrix} 0 \\ 1 \\ -1 \end{bmatrix} & \text{if } V < 0 \\ \begin{bmatrix} 1 \\ -1 \\ 0 \end{bmatrix} & \text{if } V \geq 0 \end{cases} \quad (7)$$

### 2.2.4 Diffusion Module

Diffusion involves the physical and chemical processes that disperse pollutants in the atmosphere. It's ~~is~~ influenced by meteorological conditions, i.e. atmospheric stability and humidity, and surface features, i.e. ~~land~~ land terrains and vegetation (Jiang et al., 2021). The turbulence diffusion process  $\nabla(K\nabla C_i)$  in Eq.1 helps the spread of pollutants in the atmosphere. It is expressed as the second-order deviation of species concentrations as shown in Eq. 8. They could also be discretized to convolutional operations with ~~the~~ finite difference method as shown in Eq. 9, just like that in the horizontal transport process module.

$$\nabla(K\nabla C_i) = \frac{\partial}{\partial x} \left( K \frac{\partial C_i}{\partial x} \right) + \frac{\partial}{\partial y} \left( K \frac{\partial C_i}{\partial y} \right) \quad (8)$$

$$\nabla(K\nabla C_i) = \frac{W_x * (K * W_x * C_i)}{dx \times dx} + \frac{W_y * (K * W_y * C_i)}{dy \times dy} \quad (9)$$

$$K = \text{Encoder}_K([T, RH, PRS, PBLH]) \quad (10)$$

The turbulent diffusivity  $K$  is closely related to the meteorological conditions of the atmosphere and is simulated with an encoder module  $\text{Encoder}_K$  (Eq. 10). The input variables of the  $\text{Encoder}_K$  include temperature  $T$ , humidity  $RH$ , surface pressure  $PRS$ , and boundary layer height  $PBLH$ . The  $\text{Encoder}_K$  is determined to be a grid-to-grid regression model based

on the Unet++ model with a nested structure (Zhou et al., 2018; Ronneberger et al., 2015). The *Encoder<sub>k</sub>* model consists of 5 layers with each layer respectively composed of 16, 32, 64, 128 and 256 filters.

### 2.2.5 Chemical Reaction Module

Reduced-form models like InMAP (Tessum et al., 2017) and EASIUR (Gentry et al., 2023) focus on annual-average exposure, while FastCTM provides hourly-resolved simulations critical for real-time management. FastCTM quantifies hourly contributions from individual processes (transport, chemistry, emissions) via its modular design, rather than aggregating source impacts ~~in reduced-form models~~ (e.g., EASIUR’s source-receptor matrices) ~~in reduced-form models~~). Furthermore, FastCTM explicitly couples meteorology (PBLH, T, RH) with chemistry, whereas InMAP/APEEP (Muller and Mendelsohn, 2006) assume static meteorology, ~~limiting which limits~~ their utility in capturing diurnal or synoptic-scale variations. Specifically, the air pollutant concentration changes caused by chemical reactions are represented in the following Eq. 11. In the equation, the rate of chemical reaction of species *i* is expressed as the product of a rate constant *k* and a term that is dependent on the concentrations of its reactants *j* (Carter, 1990; Carter and Atkinson, 1996).

$$R_{m,n,i,t} = k_{m,n,i,t} \times f(C_{m,n,j,t}) \quad (11)$$

$$k_i = \text{Encoder}_k([T, RH, PRS, WS, PRE, CFRAC]) \quad (12)$$

The reaction kinetics constant *k* is generally temperature-dependent. They could also be related to atmospheric pressures and moisture humidity in some reaction processes. Therefore, the reaction rate constant *k* is simulated using a spatial encoder function *Encoder* as shown in Eq. 12, which has the same structure as that of diffusion encoder modules (Eq. 10). There are 6 input variables of the *Encoder<sub>k</sub>* including *T*, *RH*, *PRS*, *WS*, *RN* and *CFRAC*. The concentration processor *f* is designed as a simple multi-layer convolutional network with a kernel size of 1 to represent high-order and complex relations among different reactants.

### 2.2.6 Deposition Module

Air pollutant deposition refers to the process by which atmospheric pollutants are transferred to Earth’s surfaces (land, water, vegetation) or removed from the air. This phenomenon plays a critical role in environmental pollution dynamics and ecosystem impacts. The deposition was closely influenced by meteorological conditions and surface characteristics (Janhäll, 2015). For example, high wind disperses pollutants, while turbulence enhances dry deposition. Forests and crops act as sinks due to large surface areas for adsorption. Air quality changes due to the deposition process are expressed linearly as the product of the deposition rate *d* and the corresponding air pollutants concentrations *C*, as shown in Eq. 13. The constant *d* is closely related to the current and previous meteorological conditions, terrains, and underlying land cover types. Therefore, they are all simulated with an *Encoder* module as shown in Eq. 14.

$$D_{m,n,i,t} = d_{m,n,i,t} \times C_{m,n,i,t} \quad (13)$$

$$d = \text{Encoder}_d([WS, RH, RN, HGT, LULC]) \quad (14)$$

The model structure and parameter configurations are also the same as that of *Encoder<sub>k</sub>* and *Encoder<sub>k</sub>*. The input data variables of *Encoder<sub>d</sub>* include WS, RH, RN, HGT and LULC.

## 2.3 Model Training

The FastCTM was programmed with ~~Python3~~Python 3 on the deep learning framework TensorFlow (Abadi et al., 2016).

The model was trained with the WRF-CMAQ operational forecast data in China for 2018–2022. Considering that on each



day we had 120-hour forecasts with a spatial coverage of  $426 \times 372$  grid cells (each with a size of  $12 \times 12 \text{ km}^2$ ) for 9 meteorological variables and  $I=10$  air pollutant variables, the total training ~~data-havedataset has~~ a size of  $\mathbf{TD} = \mathbf{R}^{1826, 120, 426, 372, 19}$ , where 1826 represents the total counting days from 2018 to 2022. Since the model was set to predict 24-hour  $\text{PM}_{2.5}$  concentrations from ~~input-1-hour input~~ data, the total input sequence length was 25 hours in each training step. Besides, the size  $M \times N$  of input data  $X_t$  to FastCTM was decided to be  $150 \times 150$ , equal to an area of  ~~$1800 \times 1800$~~   $1,800 \times 1,800 \text{ km}^2$  in 12-km resolution. Therefore, the input batch data for FastCTM in each step should be in the size of  $\mathbf{BD} = \mathbf{R}^{b, 25, 150, 150, 19}$ , where  $b$  is the batch size (determined as 1 in this study). The input data  $\mathbf{BD}$  are randomly sliced from the whole training dataset  $\mathbf{TD}$  in each training iteration, indicating each  $\mathbf{BD}$  representing different spatial and temporal coverages. The random sampling tactics ~~would-help~~ helps the model learn inherent physical and chemical principles ~~model-~~ rather than just statistical spatiotemporal autocorrelations using data in a constant spatial area (Xing et al., 2022). Besides, the spatio-temporal random samples contain varied emissions, which would improve FastCTM ~~adaption~~ adaptation to changing emission levels.

Even though five modules are defined in FastCTM, individual processes are not trained separately. The model was trained as a whole with hour-to-hour air pollutant concentrations, while each process could learn its parameters under the ~~constrains~~ constraints of its dedicated formulation. Specifically, FastCTM was tuned to minimize the loss function  $\mathcal{L}$ , which was determined to be L2 loss (Bühlmann and Yu, 2003) of the regularized mean squared error (MSE) as shown in Eq. 15. The model was optimized ~~withusing~~ the Adam optimizer (Kingma and Ba, 2014).

$$\mathcal{L} = \frac{1}{J \times N \times M \times I} \sum_{t=1}^J \sum_{m=1}^M \sum_{n=1}^N \sum_{i=1}^I (C_{m,n,i,t} - \tilde{C}_{m,n,i,t})^2 \quad (15)$$

The learning rate was set to be 0.001, and batch size to be 1. The FastCTM model was trained on one entry-level professional acceleration card of NVIDIA A40 with a running time of 10 hours for every 10000 iterations. A total of 300,000 iterations were performed ~~beforeuntil~~ the remaining model loss ~~becoming-stable~~ stabilized.

## 2.4 Model Evaluation

FastCTM ~~werewas~~ assessed against CMAQ simulations using the same input emission data and meteorological fields. ~~The Starting from 0:00 local time on each day, the~~ CMAQ model simulated 120-hour forecasts ~~from 0:00 local time on each day in one cycle. There are 139 cycles in the evaluation year of 2023, while the-~~ due to data unavailability in the remaining days. ~~The~~ FastCTM model generated 119-hour forecasts ~~withusing~~ 1-hour initial input ~~datacondition~~. The 119-hour forecasts ~~are-achieved-by-iteratively-using-an-initialized-conditionin the leading hours from the-previous step. The 119-hour forecast-data2 to 120~~ by the two models were compared ~~hour-by-hour-at-eachregarding to~~ corresponding leading time. For example, when we had 120-hour forecast starting at 0:00 on January 1, 2023 at Beijing Local Time (BLT), the data of 0:00 on January 1, 2023 were fed into FastCTM to get the 119-hour forecasts until 23:00 on January 5. The 10 species forecasts by FastCTM were compared against the CMAQ forecasts at each corresponding hour. The metrics of root mean square error (RMSE) and coefficient of determination ( $R^2$ ) were calculated daily in each of 119 leading hours on the difference in each of the 158,742 grid cells between CMAQ and FastCTM. Therefore, ~~119-static-values-for-each-metriemetrics~~ of  $R^2$  and RMSE were obtained on each lead hour at each day of the independent test year of 2023. The statistic values on each day are then averaged for the same leading hour for comparison.

The FastCTM was also assessed ~~from-the-aspectsin terms~~ of sensitivity analysis to emission inputs and meteorological fields. For meteorological variables, responses of six criteria pollutant concentrations to T, WS and PBLH were calculated. For emissions, responses to paired variables of  $\text{SO}_2/\text{NH}_4$  and  $\text{NO}_x/\text{VOC}$  ~~emissions-werewas~~ calculated. Besides,

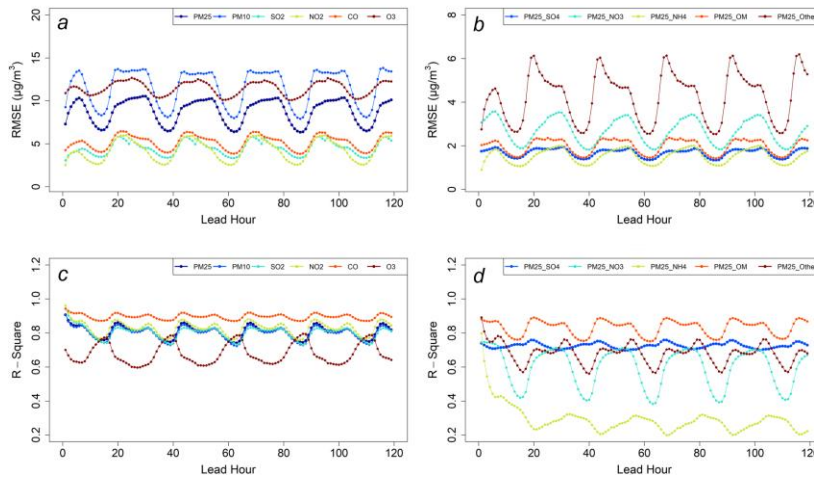


FastCTM's capability to simulate responses to emission changes were also evaluated by comparing with CMAQ simulations in 11 emission-intervention scenarios. Finally, the contributions of five internal processes of transport, diffusion, emission, reaction, and deposition were also analyzed and discussed for an example pollution episode.

### 3 Results

#### 3.1 Forecast Performance by FastCTM

The FastCTM has exhibited strong and stable strengths performance in reproducing CMAQ forecasts for a long-lasting over the 119-hour forecast period of 119 hours-evaluated infor 2023 (Figure 2). The average RMSE values for six criteria pollutants of PM<sub>2.5</sub>, PM<sub>10</sub>, SO<sub>2</sub>, NO<sub>2</sub>, CO, and O<sub>3</sub> are respectively 9.1, 11.9, 4.4, 4.0, 48.9 and 10.9 µg/m<sup>3</sup>. For R<sup>2</sup> values, they are 0.8, 0.81, 0.8, 0.83, 0.9 and 0.7. As for PM<sub>2.5</sub> components, RMSE values are 1.68, 2.68, 1.52, 1.98 and 4.25 µg/m<sup>3</sup> respectively for SO<sub>4</sub><sup>2-</sup>, NO<sub>3</sub><sup>-</sup>, NH<sub>4</sub><sup>+</sup>, organic matters and other inorganic components, while the R<sup>2</sup> values are 0.72, 0.6, 0.3, 0.83 and 0.68. Compared to the ~5ppb (~10.5 µg/m<sup>3</sup>) in the previous study by Xing et al. (2022), the FastCTM model has similar RMSE values in forecasting O<sub>3</sub>. To test the influences of initial condition on FastCTM long-term simulations, FastCTM forecasts using zero values as input air quality data were almost the same as that using ordinary input in the long leading hours. Results indicating that FastCTM simulations in long leading hours are not affected by initial conditions (Figure S5 in the SI), just like deterministic numeric-CTMs (such as CMAQ). In other words, the insensitivities of FastCTM to initial conditions indicate that it has well learned and encoded the most physical and chemical principles in CMAQ CTM, rather than just spatio-temporal correlations among air quality sequences.



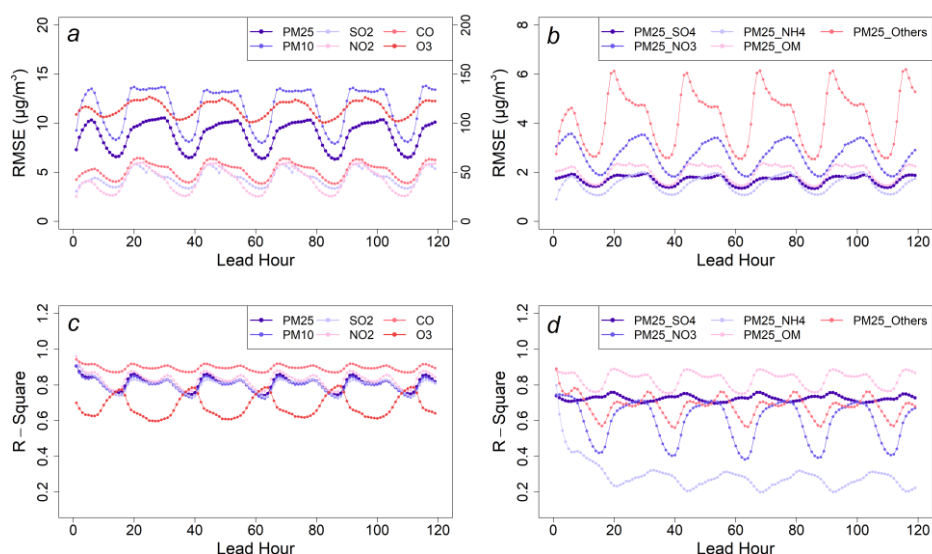


**Figure 2: The evaluation performances of FastCTM forecasts against CMAQ forecasts in 2023. Panel (a) and (b) respectively show RMSE values of criteria pollutants and the PM<sub>2.5</sub> components. Panel (c) and (d) respectively show R<sup>2</sup> values. It should be noted that RMSE value of CO corresponds to the right axis in panel (a).**

Hourly RMSE values have apparent show clear diurnal variations with lower higher RMSE values in the nighttime than that in the daytime. This is probably, which could be due to more active physical and chemical processes higher hourly concentrations of air pollutants in the daytime, which is the header to simulate nighttime except for O<sub>3</sub> (Figure S6 of SI). Consistency between CMAQ and FastCTM. Besides, since, as characterized by R<sup>2</sup>, is lower in the daytime. Since the FastCTM is a 2-D model only considering atmospheric processes within the boundary layer, lower consistency with the CMAQ model during daytime could be, possibly due to more active vigorous vertical turbulence mixing. Strong vertical mixing of air pollutants to the height above PBLH have been found (Li et al., 2017; Tang et al., 2016), which could may not be not fully represented in FastCTM. It is important to note that the relatively low R<sup>2</sup> values observed for NH<sub>4</sub><sup>+</sup>. While CMAQ explicitly resolves NH<sub>4</sub><sup>+</sup> formation reactions, FastCTM does not explicitly encode these pathways. Instead, the neural network implicitly learns relationships between NH<sub>4</sub><sup>+</sup> and precursor emissions (NH<sub>3</sub>, NO<sub>x</sub>, SO<sub>2</sub>) and meteorological variables (e.g., temperature, humidity). This simplification omits acid-base equilibria and aerosol thermodynamics, which are critical for partitioning NH<sub>4</sub><sup>+</sup> between gas and particle phases. The low R<sup>2</sup> for NH<sub>4</sub><sup>+</sup> primarily reflects FastCTM's simplified chemical mechanism in this part, which could be improved by adding related species in the simulation.

The spatial distributions of the mean absolute error (MAE) and the normalized mean absolute error (NMAE) are presented in Figure 3. For all six pollutants under consideration, it is a notable finding that the MAE values tend to be higher in polluted areas. This can be attributed to the complex and dynamic nature of pollutant interactions in such regions. In polluted environments, there are often multiple sources of emissions, complex chemical reactions, and variable meteorological conditions that can lead to greater discrepancies between the model-predicted and actual pollutant concentrations between the two models. Conversely, the NMAE values exhibit an opposite trend, being lower in polluted

设置了格式: 字体: 10 磅

设置了格式: 字体: 10 磅

设置了格式: 字体: 10 磅

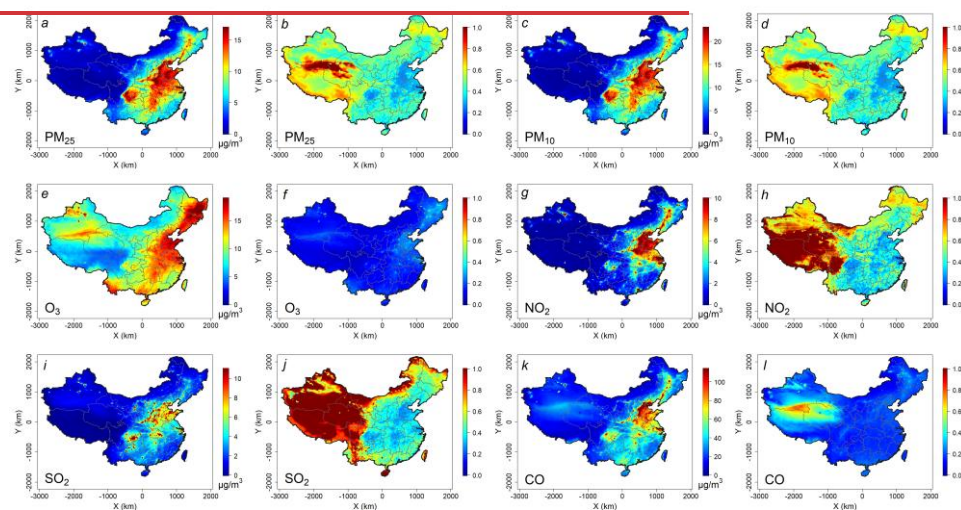
设置了格式: 字体: 10 磅

设置了格式: 字体: 10 磅

设置了格式: 字体: 10 磅

areas. In these regions, the NMAE values typically hover around 0.2, in contrast to the relatively higher values of approximately 1 in cleaner areas. The NMAE is a normalized metric that takes into account the magnitude of the actual pollutant concentrations. A lower NMAE in areas with high pollution levels suggests that the FastCTM model is effectively capturing the overall magnitude and trends of pollutant concentrations relative to the reference CMAQ model. The Air quality forecasts starting from 00:00 a.m. on March 4<sup>th</sup>, 2023 (Figure S6 in the SI) demonstrated the strong capabilities of FastCTM in modeling the complex spatio-temporal changes in a large spatial domain and over a relatively long period. In this period, air quality experienced rapid deterioration. For the pollutants except for O<sub>3</sub>, both CMAQ and FastCTM simulations have predicted very high concentrations at the 24<sup>th</sup>-hour forecast in the areas of the North China and Sichuan Basin area. During the next four days, the air quality was first cleaned up but then became worse, which was reflected both in the CMAQ and FastCTM. Generally, in this complicated process, the FastCTM generated very similar forecasts to that of the CMAQ forecasts in a long-term period over a large area. The O<sub>3</sub> generally has a close relationship with the ratio of VOCs/NO<sub>x</sub>, the increased NO<sub>2</sub> could lead to decreased O<sub>3</sub> due to titration effect (Ren and Xie, 2022) relative to the reference CMAQ simulation. The Air quality forecasts starting from 00:00 a.m. on March 4<sup>th</sup>, 2023 (Figure S7 in the SI) demonstrate FastCTM's strong capability in modelling the complex spatio-temporal changes in a large spatial domain and over a relatively long period and a large area.

设置了格式: 字体: 10 磅, 英语(美国)



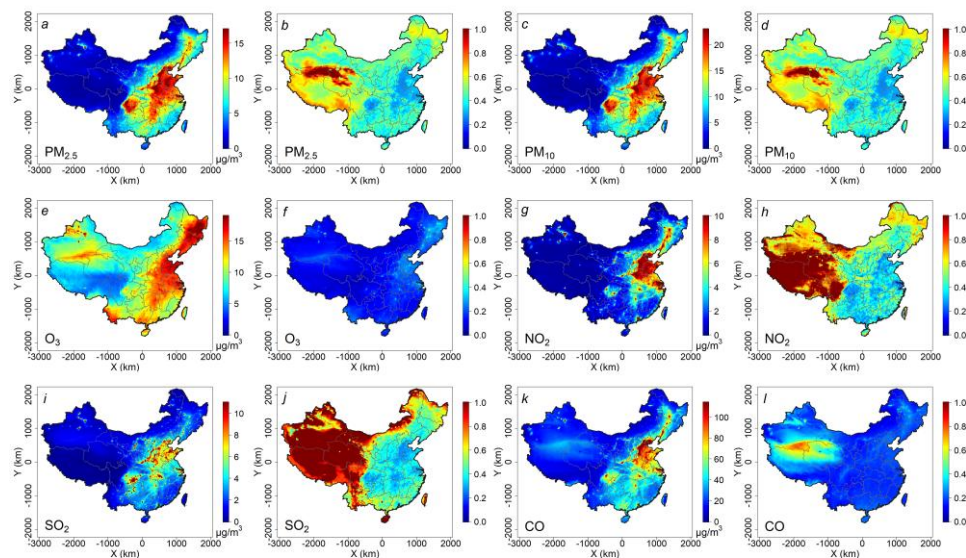


**Figure 3: Spatial distribution of mean absolute error (panels a, c, e, g, i, and k) and normalized mean absolute error for the six criteria pollutants (panels b, d, f, h, j, and l) of FastCTM ~~comparing to~~ compared with CMAQ in 2023.**

Defining the warm season as the months from April to September and the winter and cold season as the remaining months, the FastCTM model exhibited comparable performances. As shown in Figure 4 (with detailed information in Figure S7S8 in the SI), the coefficient of determination  $R^2$  values for the six criteria pollutants were 0.82, 0.8, 0.8, 0.82, 0.91, and 0.7 in the warm season, and 0.8, 0.79, 0.78, 0.83, 0.88, and 0.68 in the cold season, respectively. To assess the performance variations of FastCTM across different spatial locations, comparative evaluations were carried out in urban and rural areas as well as in inland and coastal regions. Generally, FastCTM demonstrated slightly higher accuracies in rural areas compared to urban areas (as presented in Figure S8S9 in the SI). This outcome is reasonable given the more intricate emission and chemical processes prevalent in urban settings (Guo et al., 2014). Similarly, FastCTM exhibited comparable performances in inland areas to those in coastal areas, ~~with the exception of~~ except for PM<sub>2.5</sub> and PM<sub>10</sub> (Figure S9S10 in the SI).

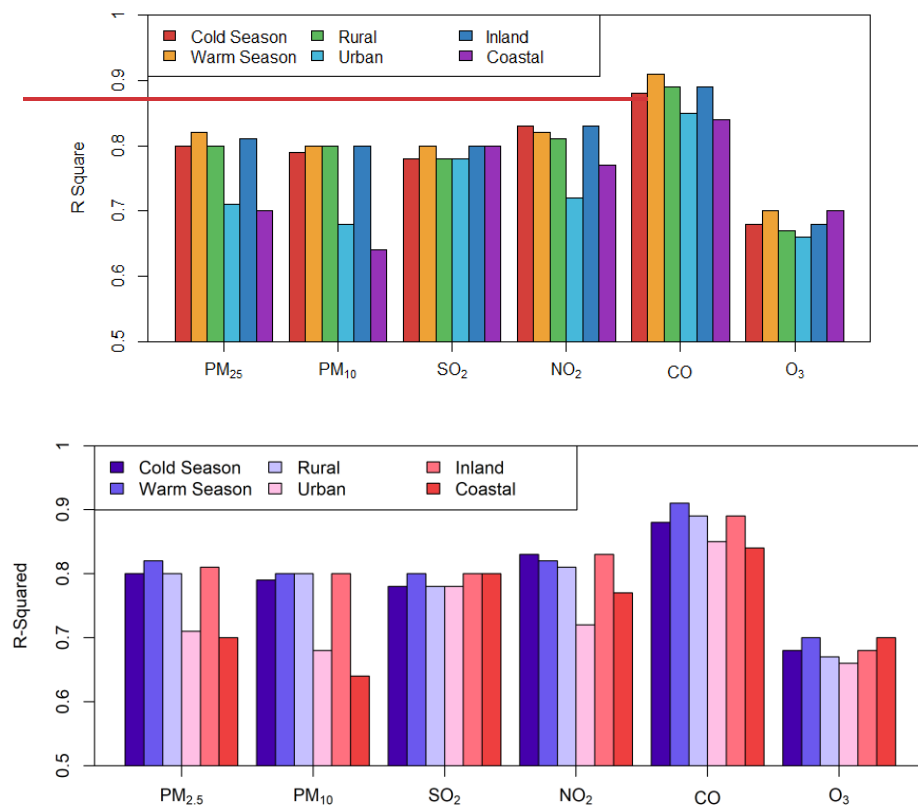


**Figure 4: The mean evaluation  $R^2$  values for all 119 leading hours of FastCTM forecasts in warm/cold seasons, rural/urban areas, and coastal/inland areas.**

To validate the FastCTM model, three land use regression (LUR) models were constructed, namely the linear regression model, the random forest model (with the number of trees set at 500), and the XGBoost model (with the booster specified as gbtrees). These LUR models were developed using the same input meteorological data, emissions, and geophysical variables as FastCTM to ensure fair comparison. When compared with the FastCTM model, the performance of the LUR models was found to be significantly inferior, as demonstrated in Table 1 and Figure S10 – S12 in the SI. For example,  $R^2$  values for FastCTM range from 0.68-0.90, whereas the LUR models only achieve 0.06-0.33. This outcome is, in fact, anticipated when we consider the complex nature of air quality dynamics: in predicting future air quality. Air quality is not a static entity, but it varies both spatially and temporally, determined by the joint effects of local emissions, meteorological conditions, and surface features, etc. For instance, the transport of air pollution is a highly dynamic process that hinges on wind fields and air pollution concentrations in a reciprocal manner. The wind direction and speed dictate the trajectory along which pollutants travel, while the existing pollutant concentrations in different regions influence the overall dispersion and mixing patterns. LUR models, which on the other hand predominantly rely on local input data (Wong et al.,

2021; Cheng et al., 2021), struggle to capture these intricate, non-local interactions. They ~~lack the capacity to~~ cannot account for the far-reaching effects, such as wind-driven pollutant transport and the ~~consequential~~ temporally accumulated changes in air quality over larger geographical areas. As far as we know, LUR models have been mostly applied in predicting air pollution fields in retrieval given corresponding air quality observations as training and constrained input data. They have been seldom used in air quality forecasts and simulations, as we have demonstrated with the FastCTM model.

**Table 1.** Performance metrics of LUR models and FastCTM compared against CMAQ

Variable	Model	RMSE	R <sup>2</sup>	NMB
<b>PM<sub>2.5</sub></b>	FastCTM	8.78	0.81	-0.15
	Liner Model	35.05	0.09	-0.24
	Random Forest	33.08	0.19	-0.25
	XGBoost	33.02	0.14	-0.12
<b>PM<sub>10</sub></b>	FastCTM	11.58	0.80	-0.17
	Liner Model	44.66	0.10	-0.23
	Random Forest	45.07	0.19	-0.33
	XGBoost	44.53	0.15	-0.21
<b>SO<sub>2</sub></b>	FastCTM	4.51	0.80	0.09
	Liner Model	39.42	0.14	-1.18
	Random Forest	25.74	0.33	-0.65
	XGBoost	25.57	0.26	-0.60
<b>NO<sub>2</sub></b>	FastCTM	4.24	0.83	0.04
	Liner Model	21.42	0.27	-0.30
	Random Forest	25.13	0.16	-0.58
	XGBoost	23.88	0.15	-0.43
<b>CO</b>	FastCTM	51.84	0.90	0.01
	Liner Model	427.67	0.03	6.38
	Random Forest	83.25	0.08	1.32
	XGBoost	70.06	0.06	1.10
<b>O<sub>3</sub></b>	FastCTM	11.46	0.68	0.02
	Liner Model	357.97	0.09	-0.46
	Random Forest	285.16	0.19	-0.21
	XGBoost	291.58	0.15	-0.22

Annually, the daily air quality typically exhibits similar fluctuations to those in other years, which can be primarily attributed to the cyclical nature of meteorological conditions and pollutant emission patterns. The FastCTM model was trained using a comprehensive dataset spanning five years, from 2018 to 2022. In light of this, it was crucial to rule out the possibility that the model was merely reproducing historical averages during the test year of 2023. To this end, the daily

national average concentrations of  $PM_{2.5}$  and  $O_3$  in 2023, as predicted by FastCTM, were meticulously compared with those simulated by CMAQ in the same test year, as well as with the CMAQ forecasts from the training years of 2018-2022. As illustrated in Figure 5, it becomes evident that the predictions made by FastCTM in 2023 align more closely with the actual CMAQ forecasts for that year, with  $R^2 = 0.94$  and  $0.72$ , respectively, for  $PM_{2.5}$  and  $O_3$ , rather than with the forecasts generated from the training data of 2018-2022. This finding, with  $R^2=0.54$  and  $0.59$ . The NMB was also lower between FastCTM and CMAQ for the same year, 2023. These results not only validates the adaptive learning capabilities of the FastCTM model but also indicates that the model is not resorting to using a simplistic approach of taking the average concentration averaging concentrations from the previous five years based on the time of day. Instead, it is likely incorporating hourly time series plots of air pollutant concentrations (Figure S6 in the SI) further demonstrate that FastCTM appears to incorporate real-time meteorological feedback, adjusting for any shifts in emission patterns, and leveraging its learned relationships to provide more accurate and contemporaneous predictions.

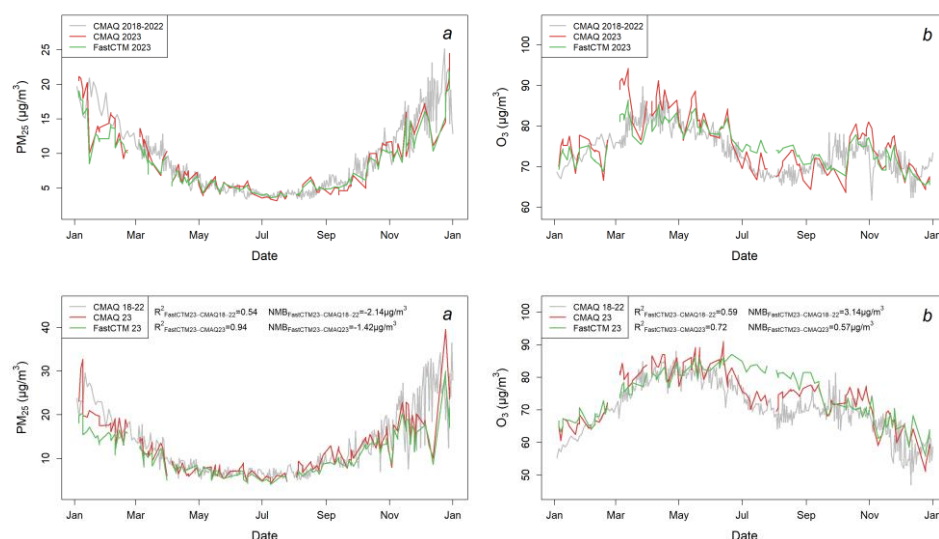


**Figure 5: The timeseries of daily FastCTM forecasts against compared with CMAQ forecasts, respectively, in training period of 2018-2022 and the evaluation period of 2023 for (a)  $PM_{2.5}$  and (b)  $O_3$ . The gaps for FastCTM and CMAQ in 2023 are due to data unavailability these days.**

### 3.2 Sensitivity Analysis with FastCTM

The FastCTM model was trained with 5-year meteorological and air quality simulations by WRF-CMAQ. These simulations used the same annual emission inventory data that was identical for each year. In this condition, the FastCTM model has learned the relationships between the air quality and varied meteorology with fixed emissions input. Considering that the FastCTM model has exhibited high accuracy at an independent evaluation year 2023, when new meteorological fields are fed into FastCTM, the deep learning model should be able to simulate responses of air pollutant concentrations to meteorological variables. However, for the response of air pollutant concentrations to emissions, the training data do not contain relationships between inter-annual varied emissions and air quality under the condition of the

设置了格式: 英语(美国)



same annual meteorological fields. Therefore, it is less expected for FastCTM to simulate reliable and correct response relationships between emissions and air quality. To validate these analyses, we calculated the sensitivities of simulated air pollutant concentrations to changes in meteorological variables and emissions.

### 3.2.1 Response of Air Pollutant Concentration to Meteorology

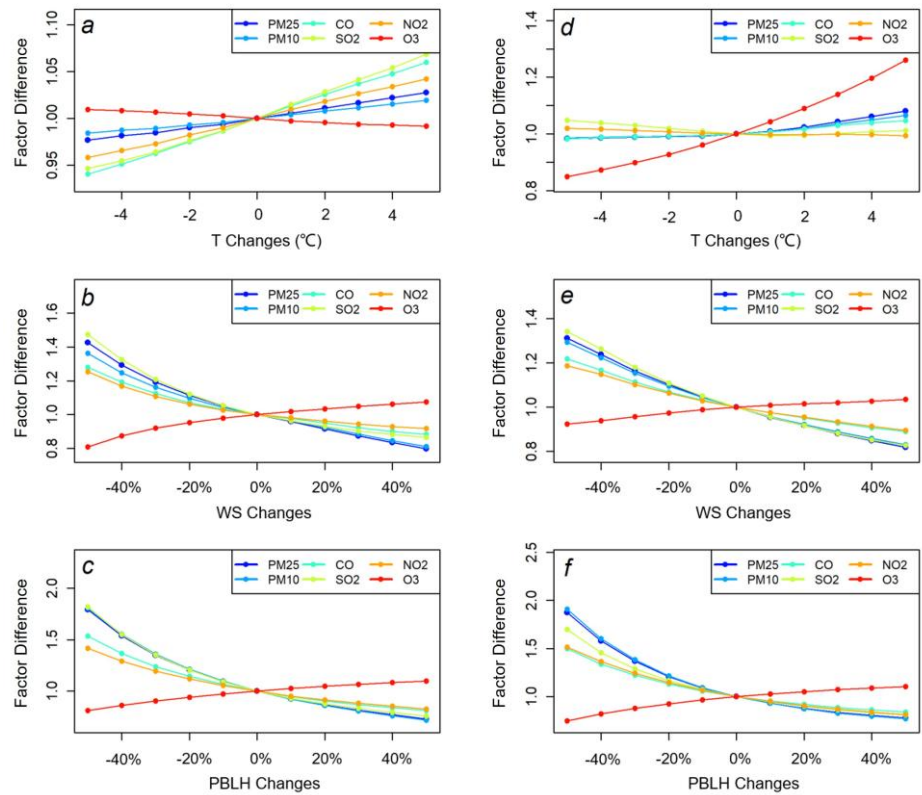


Figure 6: The FastCTM predicted air pollutant percentage changes responding to changes of T, WS, and PBLH in Beijing on January 2<sup>nd</sup> (a-c respectively in the left column) and August 1<sup>st</sup> (d-f respectively in the right column), 2023. The air pollutant concentrations are relative to those at the baseline meteorological conditions.

The responses of six criteria pollutants to meteorological changes simulated by FastCTM are evaluated as exhibited in Figure 6. For ground-level temperature (T), O<sub>3</sub> concentrations have elicited a distinct response curvature in O<sub>3</sub> concentrations compared to the other five criteria pollutants. O<sub>3</sub> concentrations have slight negative responses to T in January, as shown in Figure 6a, which is probably due to stronger dilution effects with increased NO<sub>x</sub> because higher temperatures increase NO<sub>x</sub> emissions with higher air temperature, enhancing dilution. O<sub>3</sub> concentrations had the strongest

设置了格式: 英语(美国)

设置了格式: 英语(美国)

设置了格式: 英语(美国)

设置了格式: 英语(美国)

positive responses in August among six pollutants, which is consistent with previous observation-based studies (Flaum et al., 1996). The O<sub>3</sub> had larger sensitivities when the air temperature was higher. The gaseous pollutants of CO, NO<sub>2</sub>, and SO<sub>2</sub> ~~haveshow~~ the ~~most-significantstrongest~~ positive ~~responsesresponse~~ to air temperature, which could be caused by the shift of chemical equilibrium towards ~~to~~ the higher release of these gaseous pollutants (Bassett and Seinfeld, 1983; Cox, 1982). The particulate matter pollutants, especially PM<sub>10</sub>, have the weakest responses ~~inamong~~ six pollutants. Considering that there are dominating proportions of chemically inert species in particulates, the weak responses of PM<sub>2.5</sub> and PM<sub>10</sub> are expected.

For the wind speed and PBLH, the responses of pollutants ~~are-havinghave~~ similar patterns for the same pollutant. First, O<sub>3</sub> concentrations exhibited ~~adverse-patterns contrastopposite~~ to other pollutants both in January and August. Higher wind speed would increase the dispersion and transport of air pollutants (Feng et al., 2015; Lv et al., 2017), ~~resulting in lower~~ pollution levels, ~~which is the reason for decreasedso~~ concentrations ~~along-increased-with-increasingdecrease as~~ wind speed ~~increases~~, except for O<sub>3</sub>. The contradictory response of ozone and particulate matter concentrations to PBLH is consistent with the analysis results of multiple-year observations (Liu and Tang, 2024). Theoretically, the air pollutant concentrations should exhibit an inverse relationship between air pollution concentrations and PBLH. The actual air pollutant concentration changes simulated by FastCTM generally fit the theory that there are negative ~~non-linearnonlinear~~ effects with increasing PBLH. Meanwhile, the sensitivity is stronger when the PBLH is lower (Figures 6e and 6f), which is consistent with previous observation-based analysis (Wang et al., 2019; Su et al., 2020). The totally different relationship of O<sub>3</sub> to wind speed and PBLH compared to other pollutants could be due to its high dependence on chemical precursors, such as NO<sub>x</sub> and VOC. Concentrations of these precursors could have an inverse relationship with O<sub>3</sub> at specific locations. FastCTM model itself is trained with multi-year CMAQ simulations, indicating that it is preconditioned on varied meteorological fields with the same atmospheric physical and chemical rules. Therefore, the sensitivity of air quality simulations to meteorology variations could be well learned, especially with the disciplinary-based model FastCTM.

设置了格式: 英语(美国)  
设置了格式: 英语(美国)  
设置了格式: 英语(美国)  
设置了格式: 英语(美国)

设置了格式: 英语(美国)  
设置了格式: 英语(美国)  
设置了格式: 英语(美国)  
设置了格式: 英语(美国)  
设置了格式: 英语(美国)

3.2.2 Response of Air Pollutant Concentration to Emission

The sensitivity analysis with a “brute force” method can be carried out with the FastCTM model quickly due to its high computational efficiency on GPU. The responses of PM<sub>2.5</sub> concentrations to doubled emissions of SO<sub>2</sub>, NO<sub>x</sub> were explored in a winter month of January 2023 (Figure 7). For doubled NO<sub>x</sub>, the PM<sub>2.5</sub> concentrations exhibited positive responses in most areas of China as shown in Figure 7a. ~~The most-significant-increase~~largest increases occurred in ~~regions-like~~ North China, Heilongjiang province in Northeast China, Yangtze River Delta and Sichuan province. In these places, the NO<sub>x</sub> emission are relatively large. For doubled SO<sub>2</sub>, PM<sub>2.5</sub> concentrations increased in almost all China as shown in Figure 7b. ~~The response was larger in places-of~~North China, Northeast China and Sichuan basin. ~~The PM<sub>2.5</sub> responses results of PM<sub>2.5</sub>~~ simulated by ~~the~~FastCTM ~~waswere~~ generally consistent to previous studies (Li et al., 2022).

设置了格式: 英语(美国)  
设置了格式: 英语(美国)  
设置了格式: 英语(美国)

设置了格式: 英语(美国)  
设置了格式: 英语(美国)  
设置了格式: 英语(美国)

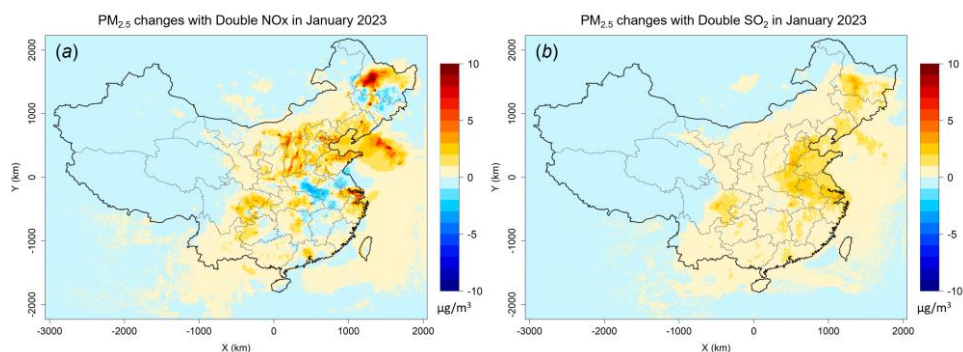


**Figure 7: Average predictions of PM<sub>2.5</sub> concentrations in 5 lead-days with doubled emissions in January 2023. Panel (a) refers to predictions with doubled NO<sub>x</sub> and panel (b) refers to double SO<sub>2</sub>.**

As for ozone, its responses to doubled NO<sub>x</sub> and VOC are explored as shown in Figure 8. For NO<sub>x</sub> emission, ~~decreased~~ ~~O<sub>3</sub>decreases in O<sub>3</sub>~~ concentrations in polluted regions like North China, ~~the~~ Yangtze River Delta, and other highly industrial regions are well ~~simulatedcaptured~~ by FastCTM. The response is reasonable considering that these regions are generally abundant with NO<sub>x</sub> emissions and at VOC-limited conditions. ~~DoubledDoubling~~ VOC ~~emission-leademissions leads to a~~ significant decrease ~~ofin~~ O<sub>3</sub> (Figure S43S14 in the supplementary material), which could be caused by the reason that increased VOC could consume O<sub>3</sub> in these regions. The spatial patterns of O<sub>3</sub> responses to NO<sub>x</sub> and VOC are similar to previous deep learning study trained by emission-controlled simulation data (Xing et al., 2022). However, due to complex speciation of VOC emissions that's simplified in the FastCTM, uncertainties for responses of O<sub>3</sub> to VOC should be noted.

设置了格式: 英语(美国)

设置了格式: 英语(美国)

设置了格式: 英语(美国)

设置了格式: 英语(美国)

设置了格式: 英语(美国)

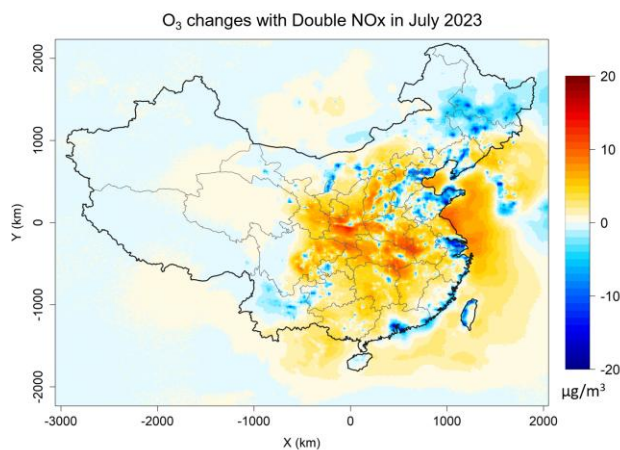


**Figure 8: Average predictions of hourly O<sub>3</sub> concentrations in 5 lead-days with doubled NO<sub>x</sub> emissions in July 2023.**

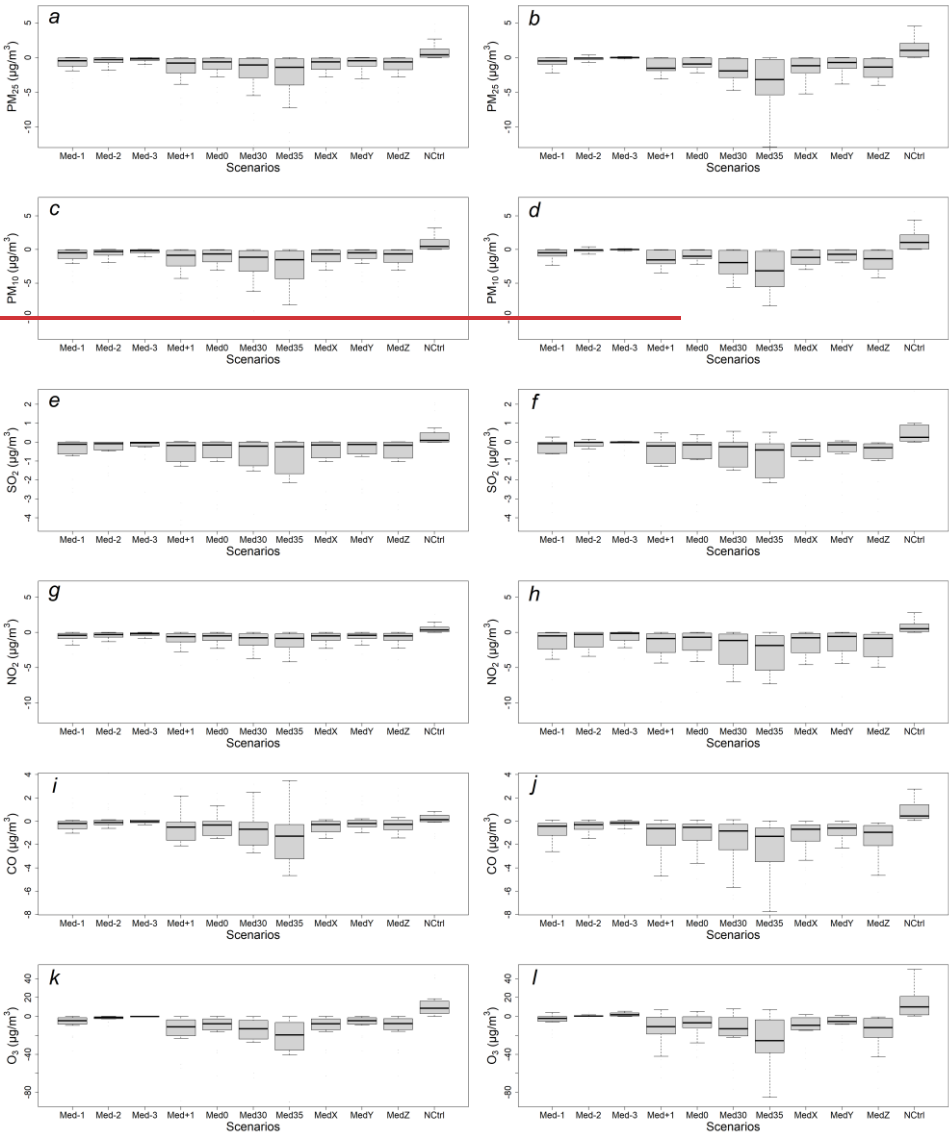
The sensitivities of FastCTM simulations to emission interventions were contrasted with those of CMAQ. Specifically, CMAQ was employed to simulate 11 emission scenarios over the two-month periods of January and July 2019 in Southwest China (Huang et al., 2022). The alterations in emissions relative to the base case are presented in Table 1. Among these scenarios, 10 involved reduced emissions of major species, with only the no-control scenario exhibiting increased emissions.

Utilizing the identical emissions and meteorological data, FastCTM also conducted simulations, which were then compared to those of CMAQ. For the 11 scenarios in question, the changes in air pollutant concentrations relative to the base case at the locations of 139 national air quality monitoring stations (Figure S14S15 in the SI) were extracted and compared in the winter month of January 2019 (Figure 99a) and in summer month of July 2019 (Figure 409b). The results indicated that, overall, the FastCTM simulations due to emissions changes were in good agreement with those of CMAQ, as reflected in two aspects. First, FastCTM predicted positive responses to increased emissions in the nocontrol (NCtrl) scenarioThe correlation coefficient R values are around 0.9 for SO<sub>2</sub>, NO<sub>2</sub>, and negative responses to other emission-controlled scenarios just as O<sub>3</sub> in both summer and winter months. For PM<sub>2.5</sub> and PM<sub>10</sub>, FastCTM exhibited higher consistency with CMAQ. Second in July than in January, with R values around 0.6 for most cases. For CO, FastCTM simulated larger air pollutanthas much better performance in January than in July, with R values of approximately 0.8 and 0.2. Considering that CO concentration decrease in those scenarios with higher emission reductions, changes are mostly due to physical dispersion and transport, the decreased performance is probably due to increased vertical mixing in summer, which is not fully represented in the 2D scheme of FastCTM. Specifically, in January 2019, with the exception of NO<sub>2</sub>, except NO<sub>2</sub>, FastCTM responded to emission changes with an interquartile range (IQR, 25% - 75% percentile) similar to that of CMAQ (Figure 9). For NO<sub>2</sub>, in the same emission reduction scenarios, FastCTM simulated lower NO<sub>2</sub> values. S16). In the summer month of July 2019, as depicted in Figure 40S17, all the criteria pollutants except CO demonstrated a comparable degree of response to emission reductions. The comparison suggests that the FastCTM model is not only capable of discerning changes in emission scenarios but can also reflect the degree of impact on air quality, thereby reinforcing its reliability and utility in simulating air quality dynamics in tandem with CMAQ. It should be noted that in both months, FastCTM exhibited slightly larger median values, suggesting its greater sensitivity to emission interventions.

**Table 2.** The emission change details of the emission scenarios

Scenario	abbreviation	Sector	NO <sub>x</sub>	VOCs	SO <sub>2</sub>	CO	PM <sub>2.5</sub>	PMC
nocontrol	NCtrl	Industrial	30%	30%	30%	30%	30%	30%
		Traffic	20%	20%	20%	20%	20%	20%
medianX	MedX	Industrial	-36%	-35%	-48%	-23%	-9%	-9%
		Traffic	-40%	-10%	0	-26%	-10%	-10%
medianY	MedY	Industrial	-26%	-20%	-38%	-13%	-4%	-4%
		Traffic	-30%	0%	0	-16%	-5%	-5%
medianZ	MedZ	Industrial	-36%	-10%	-48%	-23%	-9%	-9%
		Traffic	-40%	0%	0	-26%	-10%	-10%
median-3	Med-3	Industrial	-10%	-10%	-18%	0	0	0
		Traffic	-10%	0%	0	0	0	0
median-2	Med-2	Industrial	-16%	-20%	-28%	-3%	0	0
		Traffic	-20%	0%	0	-6%	0	0
median-1	Med-1	Industrial	-26%	-35%	-38%	-13%	-4%	-4%
		Traffic	-30%	-10%	0	-16%	-5%	-5%
median0	Med0	Industrial	-36%	-50%	-48%	-23%	-9%	-9%
		Traffic	-40%	-20%	0	-26%	-10%	-10%
median+1	Med+1	Industrial	-46%	-65%	-58%	-33%	-19%	-19%

		Traffic	-50%	-30%	0	-36%	-20%	-20%
median2030	Med30	Industrial	-55%	-70%	-80%	-40%	-40%	-40%
		Traffic	-60%	-40%	0	-40%	-40%	-40%
median2035	Med35	Industrial	-80%	-80%	-90%	-60%	-50%	-50%
		Traffic	-80%	-60%	0	-60%	-50%	-50%



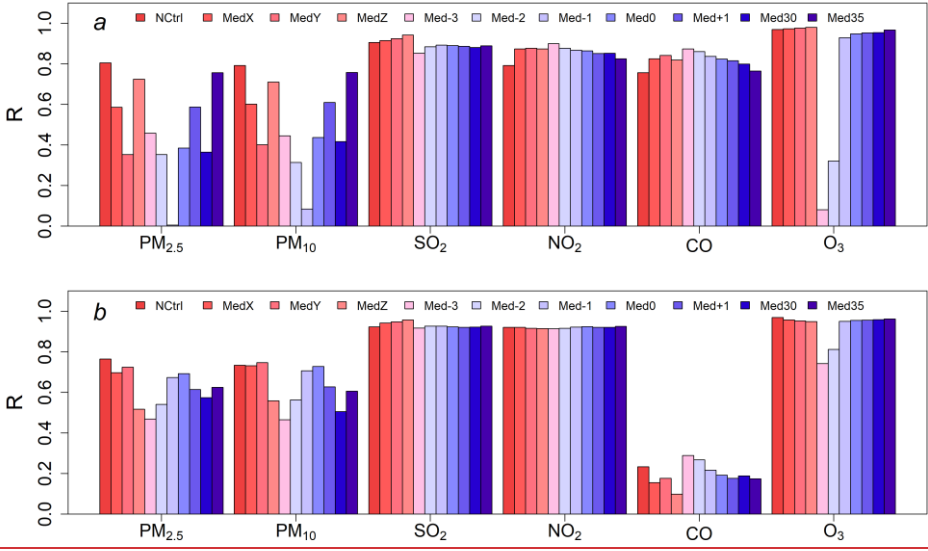


**Figure 9: Air pollutant concentration changes in terms Correlation coefficient  $R$  for responses of base case simulated by FastCTM and CMAQ (subplots of a, c, e, g, i and k in first column) to different emission scenarios and by FastCTM (subplots of b, d, f, h, j and l in second column) different air pollutants in January 2019.**

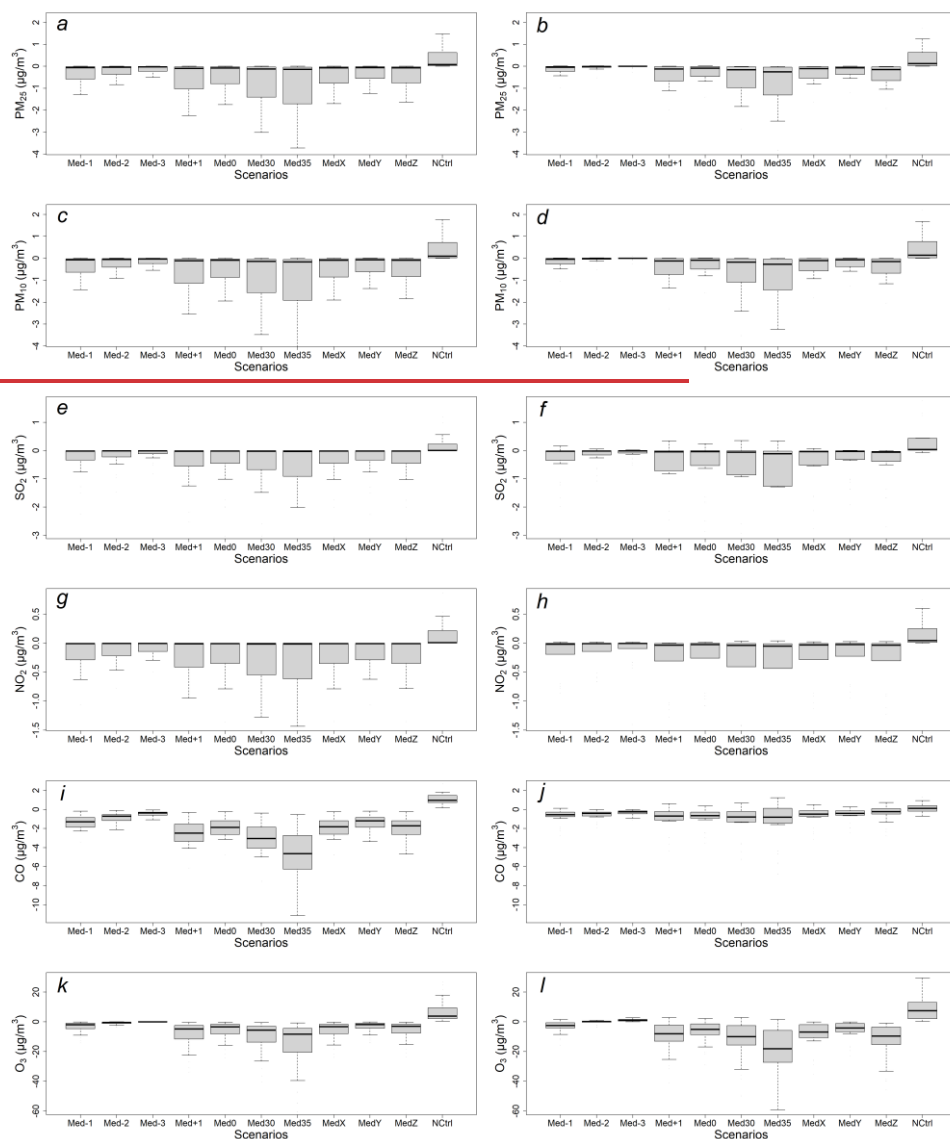


**Figure 10: Air pollutant concentration changes in terms of base case simulated by CMAQ (subplots of a, c, e, g, i, and k in the first column) and by FastCTM (subplots of b, d, f, h, j, and l in the second column) in 2023 (panel a) and July 2019, 2023 (panel b).**

FastCTM model used a principles-constrained formulation framework. As shown in Eq.4, atmospheric chemical reactions are in the Atkinson form, which independently estimate the reaction rate from meteorological conditions and polynomials of reactants concentrations in multiple powers. The principle-based formulation should be the reason for the

设置了格式



relatively significant and reasonable response simulations of PM<sub>2.5</sub> and O<sub>3</sub> to precursor emissions, even though the FastCTM itself is not trained by emission-controlled CMAQ scenario simulations. The remaining uncertainties should be attributed to the reason that FastCTM only considered environmental chemical reactants in part ~~comparing~~compared to that of ~~the~~ CMAQ model (Binkowski and Roselle, 2003).

3.3 Internal Processes Analysis with FastCTM

The FastCTM is a principles-guided deep neural network to individually simulate the dominant atmospheric physical and chemical processes as defined in Eq.1. The processes are calculated numerically with critical parameters describing the processes being estimated by deep learning encoders. The ~~hourly variations are equal to the sums of air pollutants'~~ concentration changes ~~inequal the sum of the changes produced by~~ each process. Figure 11 depicts an example during the night-time of January 13, 2023, when hourly PM<sub>2.5</sub> concentration changes significantly. Between the two hours of 18:00 and 19:00, hourly PM<sub>2.5</sub> concentrations ~~have significantly changed~~change markedly in neighbouring areas of Shandong, Hebei, and Henan provinces as shown in the red rectangle (denoted as Area A hereafter) in Figure 11c. In this example, strong northern wind prevails, leading pollutants ~~moving to move~~ southward. For PM<sub>2.5</sub> concentration changes caused by primary emissions (Figure 8d), it's ~~is~~ determined by the primary emission and the mixing volumes determined by PBLH. PM<sub>2.5</sub> changes are mostly determined by the transport process (Figure 11e) ~~sinceas~~ its spatial pattern ~~has the most resemblance to the~~closely resembles total PM<sub>2.5</sub> concentration changes. In the transport process, air pollutants move from one area to another, determined by the wind fields as shown in Eq.4. When the northern clean air prevails as in ~~the~~ Area A, changes should be negative in the upstream direction and positive in the downstream direction. The transport process simulated by FastCTM sticks to this pattern. As known to us, the diffusion process will bring pollutants from a region of high concentration to one of low concentration. Its contribution is low as shown in Figure 11f, which is reasonable considering the relatively large grid cell size of ~~12 km~~12km and short simulation period of 1 hour. PM<sub>2.5</sub> concentration changes caused by the diffusion process constituted a small proportion compared to other processes. The activities of chemical reactions are determined by both meteorological conditions and related precursor concentrations. PM<sub>2.5</sub> contribution changes between T1 and T2 caused by chemical reactions are lower in the areas to the north of Area A because the cold and clean air in this area is not favourable for chemical reactions. The deposition is the dominant process that led to PM<sub>2.5</sub> concentration reductions where regional transport was not significant. In general, ~~depositions~~deposition rates were proportional to PM<sub>2.5</sub> concentrations as shown in Figure 8h (Davis and Swall, 2006). It should be noted that FastCTM simulated air quality in a 2-D domain rather than in 3-D, the deposition ~~could~~may also include the vertical transport of air pollutants to the upper air above PBL (Zhao et al., 2020).

设置了格式: 英语(美国)

设置了格式: 英语(美国)

设置了格式: 英语(美国)

设置了格式: 英语(美国)

设置了格式: 英语(美国)

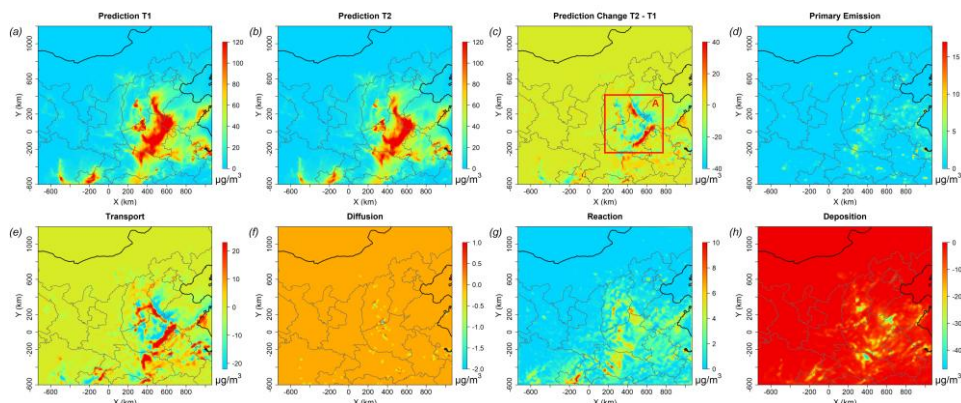
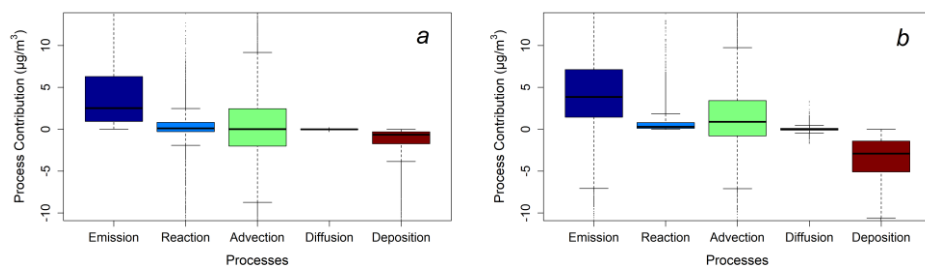
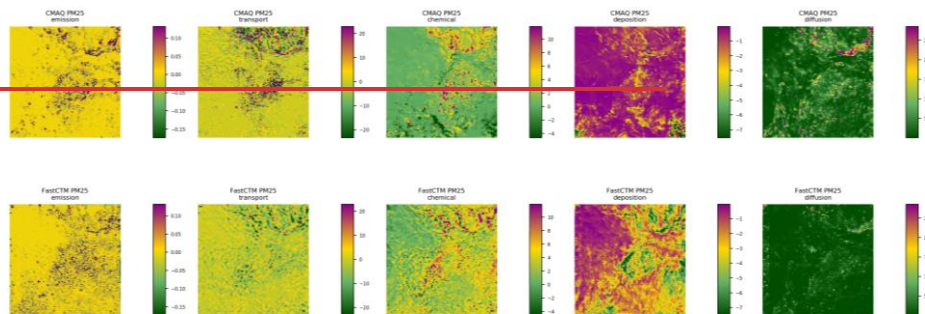


Figure 10: An example of the PM<sub>2.5</sub> concentration at T1 (18:00, panel a) and T2 (19:00, panel b) on January 13, 2023 (with the forecast leading time of 42 hours) and hourly changes (panel c). Changes caused by each of the five dominant processes are depicted in panels d-h.

In this study, we further selected the data recorded at 23:00 on October 13, 2024, to compare the impacts of the Simulated contributions of five major atmospheric physical and chemical processes, as simulated by FastCTM and CMAQ, on to hourly PM<sub>2.5</sub> concentration changes are compared between FastCTM and CMAQ at 139 stations (Figure 12). Specifically, the simulation outcomes of atmospheric S15) in the Sichuan-Chongqing region from October 12, 2024, to October 16, 2024, as shown in boxplots of Figure 11. Overall, the simulation results of the process contributions by FastCTM and its parent model CMAQ were relatively consistent. Higher degrees of consistency were found in simulations of emissions, advection processes, and diffusion processes demonstrated a relatively high degree of consistency between the two models. Regarding the simulation of Contributions from chemical reactions, while the spatial distribution of high-value areas in the FastCTM results was comparable to that of CMAQ, the simulated values in FastCTM were notably higher. Correspondingly, FastCTM overestimated the contribution of the deposition process. This exhibited overestimation counterbalanced the impact of the higher chemical reaction values. The difference in compared to CMAQ, while contributions from deposition were underestimated. The differences in the simulated deposition and reaction contributions between the two models could be due to differences in how they represent these incomplete representation of influencing factors. Overall, the simulation results of the process contributions by FastCTM and its parent model CMAQ were relatively consistent. This, given the complexity of the two processes. In general, the consistency indicates that, despite some differences in the magnitude of certain process simulations, FastCTM is capable of capturing the essential features of atmospheric processes related to PM<sub>2.5</sub> concentration changes, similar to CMAQ. Such consistency between the two models provides confidence in the reliability of FastCTM for simulating and understanding the complex interplay of atmospheric processes that govern PM<sub>2.5</sub> levels.

设置了格式: 英语(美国)



**Figure 11: An example Boxplots of contributions hourly  $PM_{2.5}$  contribution changes from five major atmospheric processes to  $PM_{2.5}$  changes ( $\mu g/m^3$ ) by CMAQ (first row) at 139 evaluation stations from October 13, 2024, to October 16, 2024, simulated by (a) CMAQ and (b) FastCTM (second row) at 23:00 on October 13, 2024.**

#### 4 Discussions

The FastCTM was a neural network-based CTM model for speeding up designed to accelerate air quality simulations and forecasts. Comparing Compared to the previous existing deep learning based CTMs, the FastCTM has offers more functionalities like akin to traditional CTM. First, it is able to simulate CTMs. It simulates 10 air pollutants, including criteria gas pollutants, coarse particulate matter, and five species concentrations of  $PM_{2.5}$ . The FastCTM has relatively high shows strong agreements in long-term forecasts with the conventional CTM. Besides, CTMs. Furthermore, after approximately two days of simulation, FastCTM simulations are not related to its predictions demonstrate independence from initial condition of input air quality fields after around two-day simulation, which indicates conditions, suggesting that the model has well successfully learned the inherent underlying physical and chemical processes mechanisms embedded in the CTM rather than only the spatial-temporal auto-correlations of input time-series data. Meanwhile simply memorizing spatiotemporal autocorrelations. Additionally, it has exhibited reasonable responses to precursor emission changes and meteorological condition changes in the sensitivity analysis. Furthermore Moreover, the internal processes in the FastCTM model were checkable are accessible and interpretable by through analyzing the contributions of dominant atmospheric chemical and physical processes separately. These processes are encoded within FastCTM by designing dedicated neural network modules.

Previous deep learning-based models for emission sensitivity analysis were generally typically trained by using simulations

with a group of different emission scenarios, whereas the FastCTM model was trained by using CMAQ simulations of unvaried annual emissions. The ~~relative reasonable responses reasonably accurate~~ simulations of responses to emissions and meteorological data ~~revealed indicate~~ that the ~~guiding principles used in formulating the behind~~ FastCTM have helped ~~the model enable it~~ to better learn the inherent physical and chemical processes within the training data. Considering the high ~~computation—computational~~ consumption by of conventional ~~CTMCTMs~~, FastCTM ~~would—reduce~~ ~~substantial~~substantially reduces computational ~~resources~~requirements.

The FastCTM has the capabilities to generate hourly pollutant simulations with nearly equal ~~aeuraies~~accuracy to ~~that those produced~~ by CMAQ-CTM, as evaluated by ~~against~~ observations at national monitoring sites. ~~There are still~~However, differences and potential errors ~~remain~~ within the FastCTM, arising from inadequate representations of actual atmospheric processes and mechanisms. First, ~~there several processes~~ are missing ~~processes were considered within the from~~ FastCTM. The chemical reactions in traditional CMAQ are ~~very highly~~ complex and ~~involves many~~involve ~~numerous~~ organic and inorganic species in gaseous and aqueous phases. The FastCTM has ~~just only~~ modeled potential chemical reactions among ~~several atmosphere compositions. Besides a limited number of atmospheric species. Additionally,~~ long-range air pollutant transport in the upper atmosphere above the planetary boundary layer was not considered within the FastCTM model. The remaining uncertainties of FastCTM compared to CMAQ could be further reduced ~~after through~~ carefully ~~detailing~~incorporating additional atmospheric processes with properly designed neural network modules.

It should also be noted that atmospheric physical and chemical processes are defined in principles-guided neural network modules in FastCTM. Their specific formulation was learned and optimized to minimize the sum of loss errors of all species concentrations, rather than being supervised by data of actual internal processes in CMAQ. The actual contributions of ~~air each process to~~ pollutant concentration changes ~~by each of these processes could can~~ be calculated ~~with using~~ the integrated process rate (IPR) analysis and integrated reaction rate (IRR) analysis tools within CMAQ. Future studies could use these IPR and IRR results to supervise the simulated processes in FastCTM to further improve its simulation ~~aeuraies~~accuracy and robustness. FastCTM may also benefit from expanded mechanisms ~~with incorporating~~ detailed gas-phase chemistry or aerosol microphysics. FastCTM's ~~design supports incremental integration of modular, principle-informed architecture facilitates targeted updates to integrate~~ additional species (e.g., ~~via user-defined modules~~ ~~without VOCs or secondary organics~~) by focusing modifications on relevant processes rather than overhauling the ~~entire~~ framework. ~~However, adding new species, especially those participating in multiple atmospheric processes, requires updating associated modules and retraining the model with the expanded set of variables to ensure the model learns the new species' interactions with existing pollutants and processes.~~ Future ~~versions~~work will explore ~~adding VOCs and secondary organics to address broader research needs such expansions, leveraging the framework's modularity to streamline updates while retraining to incorporate the new species and their dynamics.~~ FastCTM will also ~~be~~ extend to 3D dimension to improve its representation for processes such as vertical mixing, vertical wind gradient, and in-cloud ~~chemistries~~chemistry.

**Data availability.** The land use and land cover data are available at the Data Sharing and Service Portal of the Chinese Academy of Science (<http://data.casearth.cn/en/sdo/detail/5ebc2a9908415d14083a4c24>). The CTM simulation data and source code files of the exact version used to produce the results used in this paper ~~is are~~ available at <https://doi.org/10.5281/zenodo.13757211> on Zenodo (Lyu, 2024). The configuration files for running models of WRF v3.4.1 and CAMQ v5.0.2 are also available at <https://doi.org/10.5281/zenodo.5152621> (Hu, 2021).

**Author contributions.** BL and YH conceived the study. BL developed the model and codes. RH and XW contributed the CTM simulation data. BL and RH collected the observation data. BL analyzed data and wrote the paper with contributions from YH, RH, WW, and XW. RH managed the project.

**Competing interests.** The authors declare that they have no conflict of interest.

**Acknowledgements.** This research has been in part supported by the AiMa R&D Project (R#2016-004) of Hangzhou AiMa Technologies. The findings in this research do not necessarily reflect the views of the sponsors.

**Reference**

Abadi, M., Agarwal, A., Barham, P., Brevdo, E., Chen, Z., Citro, C., Corrado, G. S., Davis, A., Dean, J., and Devin, M.:  
Tensorflow: Large-scale machine learning on heterogeneous distributed systems, arXiv preprint arXiv:1603.04467,  
2016.

Appel, K. W., Napelenok, S. L., Foley, K. M., Pye, H. O., Hogrefe, C., Luecken, D. J., Bash, J. O., Roselle, S. J., Pleim, J.  
E., and Foroutan, H.: Description and evaluation of the Community Multiscale Air Quality (CMAQ) modeling system  
version 5.1, Geoscientific model development, 10, 1703-1732, 2017.

Bassett, M. and Seinfeld, J. H.: Atmospheric equilibrium model of sulfate and nitrate aerosols, Atmospheric Environment  
(1967), 17, 2237-2252, [https://doi.org/10.1016/0004-6981\(83\)90221-4](https://doi.org/10.1016/0004-6981(83)90221-4), 1983.

Binkowski, F. S. and Roselle, S. J.: Models-3 Community Multiscale Air Quality (CMAQ) model aerosol component 1.  
Model description, Journal of Geophysical Research Atmospheres, 108, 335-346, 2003.

Bühlmann, P. and Yu, B.: Boosting With the L2 Loss, Publications of the American Statistical Association, 98, 324-339,  
2003.

Byun, D. and Schere, K. L.: Review of the governing equations, computational algorithms, and other components of the  
Models-3 Community Multiscale Air Quality (CMAQ) modeling system, Applied Mechanics Reviews, 59, 51-77,  
2006.

Carter, W. P. L.: A detailed mechanism for the gas-phase atmospheric reactions of organic compounds, Atmospheric  
Environment. Part A. General Topics, 24, 481-518, [https://doi.org/10.1016/0960-1686\(90\)90005-8](https://doi.org/10.1016/0960-1686(90)90005-8), 1990.

Carter, W. P. L. and Atkinson, R.: Development and evaluation of a detailed mechanism for the atmospheric reactions of  
isoprene and NOx, International Journal of Chemical Kinetics, 28, 497-530, [https://doi.org/10.1002/\(SICI\)1097-4601\(1996\)28:7<497::AID-KIN4>3.0.CO;2-Q](https://doi.org/10.1002/(SICI)1097-4601(1996)28:7<497::AID-KIN4>3.0.CO;2-Q), 1996.

Cheng, B., Ma, Y., Feng, F., Zhang, Y., Shen, J., Wang, H., Guo, Y., and Cheng, Y.: Influence of weather and air pollution  
on concentration change of PM2.5 using a generalized additive model and gradient boosting machine, Atmospheric  
environment, 255, 118437, 2021.

Council, N.: Air quality management in the United States, National Academies Press 2004.

Cox, R. A.: Chemical Transformation Processes for NoX Species in the Atmosphere, in: Studies in Environmental Science,  
edited by: Schneider, T., and Grant, L., Elsevier, 249-261, <https://doi.org/10.1016/B978-0-444-42127-2.50027-0>,  
1982.

Davis, J. M. and Swall, J. L.: An examination of the CMAQ simulations of the wet deposition of ammonium from a

带格式的: 行距: 1.5 倍行距, 不对齐到网格

Bayesian perspective, *Atmospheric Environment*, 40, 4562-4573, 2006.

Eder, B., Kang, D., Mathur, R., Yu, S., and Schere, K.: An operational evaluation of the Eta-CMAQ air quality forecast model, *Atmospheric Environment*, 40, 4894-4905, 2006.

Efstathiou, C. I., Adams, E., Coats, C. J., Zelt, R., Reed, M., McGee, J., Foley, K. M., Sidi, F. I., Wong, D. C., and Fine, S.: Enabling high-performance cloud computing for the Community Multiscale Air Quality Model (CMAQ) version 5.3.3: performance evaluation and benefits for the user community, *Geoscientific Model Development*, 17, 7001-7027, 2024.

Feng, X., Li, Q., Zhu, Y., Hou, J., Jin, L., and Wang, J.: Artificial neural networks forecasting of PM<sub>2.5</sub> pollution using air mass trajectory based geographic model and wavelet transformation, *Atmospheric Environment*, 107, 118-128, <http://dx.doi.org/10.1016/j.atmosenv.2015.02.030>, 2015.

Flaum, J. B., Rao, S. T., and Zurbenko, I. G.: Moderating the Influence of Meteorological Conditions on Ambient Ozone Concentrations, *Journal of the Air & Waste Management Association* (1995), 46, 35-46, 1996.

Gentry, B. M., Robinson, A. L., and Adams, P. J.: EASIUR-HR: a model to evaluate exposure inequality caused by ground-level sources of primary fine particulate matter, *Environmental Science & Technology*, 57, 3817-3824, 2023.

Hakami, A., Odman, M. T., and Russell, A. G.: High-Order, Direct Sensitivity Analysis of Multidimensional Air Quality Models, *Environmental Science & Technology*, 37, 2442-2452, 10.1021/es020677h, 2003.

He, K., Zhang, X., Ren, S., and Sun, J.: Deep Residual Learning for Image Recognition, *IEEE*, 2016.

Huang, L., Liu, S., Yang, Z., Xing, J., and Liu, T. Y.: Exploring Deep Learning for Air Pollutant Emission Estimation, *Geoscientific Model Development*, 14, 4641-4654, 2021.

HUANG, R., WANG, X., WANG, C., DU, Y., YAN, B., ZHANG, W., LUO, B., ZHANG, W., and HU, Y.: Future Year Air Quality Attainment Prediction Method Based on Design&nbsp;Value and Relative Response Factor: A Case Study Focusing on Implementation Planning of the 14th Five-Year Plan in Sichuan Province, *Acta Scientiarum Naturalium Universitatis Pekinensis*, 58, 553-564, 2022.

Irrgang, C., Boers, N., Sonnewald, M., Barnes, E. A., Kadow, C., Staneva, J., and Saynisch-Wagner, J.: Towards neural Earth system modelling by integrating artificial intelligence in Earth system science, *Nature Machine Intelligence*, 3, 667-674, 10.1038/s42256-021-00374-3, 2021.

Janhäll, S.: Review on urban vegetation and particle air pollution-Deposition and dispersion, *Atmospheric environment*, 105, 130-137, 2015.

Jiang, Z., Cheng, H., Zhang, P., and Kang, T.: Influence of urban morphological parameters on the distribution and diffusion of air pollutants: A case study in China, *Journal of Environmental Sciences*, 105, 163-172, 2021.

Kelp, M. M., Jacob, D. J., Lin, H., and Sulprizio, M. P.: An online-learned neural network chemical solver for stable long-term global simulations of atmospheric chemistry, *Journal of Advances in Modeling Earth Systems*, 14, e2021MS002926, 2022.

Kingma, D. and Ba, J.: Adam: A Method for Stochastic Optimization, *Computer Science*, 2014.

Lang, J.: A Monitoring and Modeling Study to Investigate Regional Transport and Characteristics of PM<sub>2.5</sub> Pollution, *Aerosol & Air Quality Research*, 13, 943-956, 2013.

Leal, A. M., Kulik, D. A., Smith, W. R., and Saar, M. O.: An overview of computational methods for chemical equilibrium and kinetic calculations for geochemical and reactive transport modeling, *Pure and Applied Chemistry*, 89, 597-643, 2017.

LeCun, Y., Bengio, Y., and Hinton, G.: Deep learning, *Nature*, 521, 436-444, 10.1038/nature14539, 2015.

Li, J., Dai, Y., Zhu, Y., Tang, X., Wang, S., Xing, J., Zhao, B., Fan, S., Long, S., and Fang, T.: Improvements of response surface modeling with self-adaptive machine learning method for PM<sub>2.5</sub> and O<sub>3</sub> predictions, *Journal of Environmental Management*, 303, 114210, <https://doi.org/10.1016/j.jenvman.2021.114210>, 2022.

Li, Z., Guo, J., Ding, A., Liao, H., Liu, J., Sun, Y., Wang, T., Xue, H., Zhang, H., and Zhu, B.: Aerosol and boundary-layer interactions and impact on air quality, *National Science Review*, 4, 810-833, 2017.

Liao, Q., Zhu, M., Wu, L., Pan, X., Tang, X., and Wang, Z.: Deep Learning for Air Quality Forecasts: a Review, *Current Pollution Reports*, 6, 399-409, 10.1007/s40726-020-00159-z, 2020.

Liu, X.-H., Zhang, Y., Xing, J., Zhang, Q., Wang, K., Streets, D., Jang, C., Wang, W.-X., and Hao, J.-M.: Understanding of regional air pollution over China using CMAQ, Part II. Process analysis and sensitivity of ozone and particulate matter to precursor emissions, *Atmospheric Environment*, 44, 3719-3727, 10.1016/j.atmosenv.2010.03.036, 2010.

Liu, Y. and Tang, G.: Contradictory response of ozone and particulate matter concentrations to boundary layer meteorology, *Environmental Pollution*, 343, 123209, <https://doi.org/10.1016/j.envpol.2023.123209>, 2024.

Liu, Z.-S., Clusius, P., and Boy, M.: Neural network emulator for atmospheric chemical ODE, *Neural Networks*, 184, 107106, 2025.

Lv, B., Cai, J., Xu, B., and Bai, Y.: Understanding the Rising Phase of the PM<sub>2.5</sub> Concentration Evolution in Large China Cities, *Scientific Reports*, 7, 46456, 10.1038/srep46456 <https://www.nature.com/articles/srep46456#supplementary-information>, 2017.

Mao, W., Wang, W., Jiao, L., Zhao, S., and Liu, A.: Modeling air quality prediction using a deep learning approach: Method optimization and evaluation, *Sustainable Cities and Society*, 65, 102567, <https://doi.org/10.1016/j.scs.2020.102567>, 2021.

Michalakes, J., Chen, S., Dudhia, J., Hart, L., Klemp, J., Middlecoff, J., and Skamarock, W.: Development of a next-generation regional weather research and forecast model, *IEEE International Conference on High Performance Computing, Data, and Analytics*, 11/1/2001, 10.1142/9789812799685\_0024, 2001.

Michalakes, J., Dudhia, J., Gill, D., Henderson, T., Klemp, J., Skamarock, W., and Wang, W.: The Weather Research and Forecast Model: Software Architecture and Performance, 10.1142/9789812701831\_0012, -2005.

Muller, N. Z. and Mendelsohn, R.: The air pollution emission experiments and policy analysis model (APEEP) technical appendix, Yale University: New Haven, CT, USA, 1, 2006.

Reichstein, M., Camps-Valls, G., Stevens, B., Jung, M., Denzler, J., Carvalhais, N., and Prabhat: Deep learning and process understanding for data-driven Earth system science, *Nature*, 566, 195-204, 10.1038/s41586-019-0912-1, 2019.

Ren, J. and Xie, S.: Diagnosing ozone-NO<sub>x</sub>-VOC sensitivity and revealing causes of ozone increases in China based on 2013–2021 satellite retrievals, 10.5194/aep-2022-347, 2022.

Ronneberger, O., Fischer, P., and Brox, T.: U-Net: Convolutional Networks for Biomedical Image Segmentation, *Medical Image Computing and Computer-Assisted Intervention – MICCAI 2015*, Cham, 2015//, 234-241,

Shi, X., Chen, Z., Wang, H., Yeung, D.-Y., Wong, W.-k., and Woo, W.-c.: Convolutional LSTM Network: A Machine Learning Approach for Precipitation Nowcasting, *Computer Science*, 2015.

Shi, X., Gao, Z., Lausen, L., Wang, H., Yeung, D. Y., Wong, W., and Woo, W.: Deep Learning for Precipitation Nowcasting: A Benchmark and A New Model, 2017.

Silva, S. J., Heald, C. L., Ravela, S., Mammarella, I., and Munger, J. W.: A deep learning parameterization for ozone dry deposition velocities, *Geophysical Research Letters*, 46, 983-989, 2019.

Skamarock, W. C., Klemp, J. B., Dudhia, J., Gill, D. O., Barker, D. M., Duda, M. G., Huang, X. Y., Wang, W., and Powers,



J. G.: A description of the advanced research WRF version 3, NCAR Tech. Note 2008., 2008.

Sturm, P. O. and Wexler, A. S.: A mass- and energy-conserving framework for using machine learning to speed computations: a photochemistry example, *Geoscientific Model Development*, 13, 4435–4442, 2020.

Su, T., Li, Z., Zheng, Y., Luan, Q., and Guo, J.: Abnormally Shallow Boundary Layer Associated With Severe Air Pollution During the COVID-19 Lockdown in China, *Geophysical Research Letters*, 10.1029/2020GL090041, 2020.

Sum, H., Fung, J. C. H., Chen, Y., Li, Z., Yuan, D., Chen, W., and Lu, a. X.: Development of an LSTM broadcasting deep-learning framework for regional air pollution forecast improvement, *Geosci. Model Dev.*, 15, 8439–8452, 2022.

Tang, G., Zhang, J., Zhu, X., Song, T., Munkel, C., Hu, B., Schäfer, K., Liu, Z., Zhang, J., and Wang, L.: Mixing layer height and its implications for air pollution over Beijing, China, *Atmospheric Chemistry and Physics*, 16, 2459–2475, 2016.

Tessum, C. W., Hill, J. D., and Marshall, J. D.: InMAP: A model for air pollution interventions, *PLOS ONE*, 12, e0176131, 10.1371/journal.pone.0176131, 2017.

Wang, C., Jia, M., Xia, H., Wu, Y., Wei, T., Shang, X., Yang, C., Xue, X., and Dou, X.: Relationship analysis of PM<sub>2.5</sub> and boundary layer height using an aerosol and turbulence detection lidar, *Atmospheric Measurement Techniques*, 12, 3303–3315, 10.5194/amt-12-3303-2019, 2019.

Wang, L., Jang, C., Zhang, Y., Wang, K., Zhang, Q., Streets, D., Fu, J., Lei, Y., Schreifels, J., He, K., Hao, J., Lam, Y.-F., Lin, J., Meskhidze, N., Voorhees, S., Everts, D., and Phillips, S.: Assessment of air quality benefits from national air pollution control policies in China. Part II: Evaluation of air quality predictions and air quality benefits assessment, *Atmospheric Environment*, 44, 3449–3457, <http://dx.doi.org/10.1016/j.atmosenv.2010.05.058>, 2010.

Wang, Y., Gao, Z., Long, M., Wang, J., and Yu, P. S.: PredRNN++: Towards A Resolution of the Deep-in-Time Dilemma in Spatiotemporal Predictive Learning, 2018.

Wong, P.-Y., Lee, H.-Y., Chen, Y.-C., Zeng, Y.-T., Chern, Y.-R., Chen, N.-T., Lung, S.-C. C., Su, H.-J., and Wu, C.-D.: Using a land use regression model with machine learning to estimate ground level PM<sub>2.5</sub>, *Environmental Pollution*, 277, 116846, 2021.

Xia, Z., Zhao, C., Du, Q., Yang, Z., Shuai, Z. M., and Liang, Q.: Advancing Photochemistry Simulation in WRF-Chem V4.0: Artificial Intelligence PhotoChemistry (AIPC) Scheme with Multi-Head Self-Attention Algorithm, -2024.

Xing, J., Zheng, S., Li, S., Huang, L., Wang, X., Kelly, J. T., Wang, S., Liu, C., Jang, C., Zhu, Y., Zhang, J., Bian, J., Liu, T.-Y., and Hao, J.: Mimicking atmospheric photochemical modeling with a deep neural network, *Atmospheric Research*, 265, 105919, <https://doi.org/10.1016/j.atmosres.2021.105919>, 2022.

Zhang, X., Liu, L., Chen, X., Gao, Y., Xie, S., and Mi, J.: GLC\_FCS30: Global land-cover product with fine classification system at 30 m using time-series Landsat imagery, *Earth System Science Data Discussion*, <https://doi.org/10.5194/essd-2020-182>, 2020.

Zhang, Z., Zhang, S., Chen, C., and Yuan, J.: A systematic survey of air quality prediction based on deep learning, *Alexandria Engineering Journal*, 93, 128–141, <https://doi.org/10.1016/j.aej.2024.03.031>, 2024.

Zhao, J., Ma, X., Wu, S., and Sha, T.: Dust emission and transport in Northwest China: WRF-Chem simulation and comparisons with multi-sensor observations, *Atmospheric Research*, 241, 104978, <https://doi.org/10.1016/j.atmosres.2020.104978>, 2020.

Zhou, Z., Rahman Siddiquee, M. M., Tajbakhsh, N., and Liang, J.: UNet++: A Nested U-Net Architecture for Medical Image Segmentation, *Cham*, 3–11,